Patrik Nyberg

# Evaluation of heat transfer from diesel spray combustion using a heat flux sensor in an optical chamber

School of Technology and Innovations
Master's thesis in Science
Energy Technology

Vaasa 2024

ACKNOWLEDGEMENTS

This thesis has been done for Wärtsilä Finland Oyj, Research and Technology development department. I am thankful for my instructor, Jari Hyvönen at Wärtsilä for this opportunity and for the support during this work. I also express my gratitude to University of Vaasa and my supervisor Seppo Niemi for being helpful and enabling the extended work in this thesis.

A special thank you to Andrey Mityakov who provided the sensors used in this thesis and whose expertise was indispensable. In kind to Tomi Riiki who provided support when needed during instrumentation work.

I am grateful to the spray chamber team consisting of Viljam Grahn, Roberth Sjöström, Joonas Koivuluoma, Mikko Lähteenmäki, Eddie Westerlund, Lokesh Mopuri. Work we did is something I am still proud of and remember fondly. Many thanks to Viljam, with whom we shared knowledge and assisted each other in doing our own work. I greatly appreciate what we did together. I give thanks to Ahmad Zeeshan and Cheng Qiang who assisted during the measurement campaign, and to Dave Lowe and Gavin Sutton who provided the pyrometer.

Special thanks to family and friends who provided support while completing my master's thesis. I am especially thankful to Susanna, for being understanding to the long days working on this thesis

Vaasa, December 2024

Patrik Nyberg

**UNIVERSITY OF VAASA**
**School of Technology and Innovations**
**Author:** Patrik Nyberg
**Title of the thesis:** Evaluation of heat transfer from diesel spray combustion using a heat flux sensor in an optical chamber
**Degree:** Master of Sciences
**Discipline:** Energy Technology
**Supervisor:** Professor Seppo Niemi
**Instructor:** D.Sc. Jari Hyvönen
**Year:** 2024 **Pages:** 88

**ABSTRACT :**
This thesis was requested by Wärtsilä's Research and Technology Development department to provide measurement data for Computational Fluid Dynamic modules to conjugate heat transfer analysis on fuel injector spray combustion. An Optical Spray Combustion Chamber was used for measurement, to replicate the environment of engine combustion chambers. Additionally, it was possible to record visual data during the spray combustion sequence. Other measurements were performed in parallel to provide additional data for this measurement campaign. These data include spectrometry, pyrometry, phosphor thermometry, and both monochromatic and color pictures using high-speed cameras.

Method of measuring heat transfer was with Gradient Heat Flux Sensor capable of measuring heat flux through the sensor. The goal of this thesis was to design installation methodology for sensors capable of withstanding repeating combustion sprays. Preparation of components with sensors is discussed in detail. Measurement setup planned was to have combustion spray hitting a flat surface where sensors would be installed. This simple setup would be then replicated with future simulation models. Gathered data would be used to assess the performance of the model.

Instrumentation method used to install sensors inside the combustion chamber showed two main problems. Firstly, the Instrumented corner modules installed to the combustion chamber broke during initial testing. Damage was caused by the pre-combustion sequence. Pre-combustion sequence is used to provide correct gas mixture and pressure inside the chamber. Adhesive layer broke down from the detonation wave hitting the sensor. The second important problem faced was with signal noise from ground loop. Due to the noise pre-calibration work done on sensors could not be used.

Sensors installed on the instrumented plate were able to survive 30 combustion sequences. These included 30 pre-combustions and 15 spray combustions hitting the plate. Eleven measurements were able to be used to measure an average heat flux. Due to the noise signal recalibration was required. New sensitivity was calculated from surface temperature on the instrumented plate. Phosphor thermometry was used to measure an average temperature. Measurement point was at 11 ms after Start of Energization of the injector. Data recorded showed that 880 K was reached during that moment. Heat flux during the spray combustion sequence was calculated from these results. Peak heat flux was estimated to be between 2 – 3.5 $MW/m^2$ or 4.5 – 8 $MW/m^2$ depending on the assumed peak surface temperature.

**KEYWORDS:** Diesel spray combustion, heat transfer, heat flux, heat measurement method, sensor instrumentation

**VAASAN YLIOPISTO**
**Tekniikan ja innovaatiojohtamisen yksikkö**
**Tekijä:** Patrik Nyberg
**Diplomityön nimi:** Dieselin ruiskutuksen lämpövirran arviointi lämpövuoanturilla optisessa palamiskammiossa
**Tutkinto:** Diplomi-insinööri
**Oppiaine:** Energiatekniikka
**Työn valvoja:** Seppo Niemi Professori
**Työn ohjaaja:** Jari Hyvönen TkT
**Valmistumisvuosi:** 2024 **Sivumäärä:** 88

**TIIVISTELMÄ:**
Tämä diplomityö on tehty Wärtsilän Tutkimus- ja Teknologiakehitysosastolle tarjoamaan mittausdataa laskennallisten virtausdynamiikkamoduulien käyttöön. Tutkimuskohteena oli moottorin suuttimen aiheuttama lämpövirta palamiskammiossa. Mittaukset suoritettiin optisessa palamiskammiossa, joka jäljitteli moottorin palotilaolosuhteita. Palamiskammio mahdollisti palamisen visuaalisen tallennuksen. Muita mittauksia tehtiin mittauskampanjan aikana spektrometrillä, pyrometrillä, valomonistinputkella lämpötilan mittaukseen fosforipinnasta sekä suurnopeuskameroilla.

Lämpövirta mitattiin Gradient Heat Flux -sensorin avulla, joka pystyi mittaamaan lämpövuon anturin läpi. Työn tavoite oli suunnitella anturin asennusmenetelmä, joka kestäisi toistuvia palamistapahtumia. Työhön kuului antureiden instrumentointi mittauskomponentteihin. Päämittaustavoite oli saada suuttimen suihku osumaan instrumentoituun levyyn. Levyn pinta oli sileä simulaatiomallin yksinkertaistamiseksi. Kerättyä dataa käytettäisiin mallien toimivuuden arvioimiseen.

Antureiden asentamisessa palamiskammioon ilmeni kaksi pääongelmaa. Palotilaan asennetut instrumentoidut kulmamoduulit rikkoutuivat ennen palamistapahtumaa. Pääsyynä oli kammiossa tehty esipalaminen. Esipalamista käytetään oikean kaasuseoksen ja paineen saavuttamiseksi kammiossa. Anturin ja komponentin välinen liimakerros petti esipalamisen aiheuttaman räjähdysaallon vaikutuksesta. Toinen havaittu ongelma oli antureihin kohdistuva signaalihäiriö. Signaalihäiriön takia antureiden kalibrointeja ei voitu mittauksissa käyttää.

Instrumentoidulle levylle asennetut anturit kestivät 30 palamisjaksoa. Näihin sisältyi 30 esipalamista ja 15 varsinaista palamista. Näistä mittauksista 11 pystyttiin käyttämään keskimääräisen lämpövuon mittaukseen. Anturit uudelleenkalibrointiin signaalimelun takia. Antureiden uusi signaaliherkkyys laskettiin instrumentoidun levyn mitatusta pintalämpötilasta. Lämpötila 880 K mitattiin 11 ms suuttimen käynnistyshetken jälkeen. Palamisen lämpövuo laskettiin tämän tuloksen avulla. Laskettu huippulämpövuo oli 2 – 3.5 $MW/m^2$ tai 4.5 – 8 $MW/m^2$ välillä riippuen instrumentointilevyn huippupintalämpötilasta.

**AVAINSANAT:** Dieselpalaminen, lämpövuo, lämpövirta, lämpövuon mittaaminen, anturin instrumentointi

## Contents

## Figures

## Tables



## Abbreviations

| | |
|---|---|
| δ | Sensor thickness |
| $\partial T$ | Temperature difference |
| $\partial x$ | Length difference along the x-axis |
| ∇T | Temperature gradient |
| $\nabla T_z$ | Projection of temperature gradient onto the z axis. |
| $\theta_{opt}$ | Optimal cut angle |
| A | Area of the Anisotropic thermoelement |
| b | Width of the Anisotropic thermoelement |
| $C_1$ | Crystallographic axis 1 |
| $C_2$ | Crystallographic axis 2 |
| $C_3$ | Crystallographic axis 3 |
| d | Diameter of the nickel foil tube |
| ê | Seebecks coefficient |
| E | Measured Voltage output |
| $\overrightarrow{E_{\|\|}}$ | Thermopower |

| | |
|---|---|
| $\overrightarrow{E_{\perp}}$ | Electronic vector |
| $E_x$ | Thermo-Electromotive Force in the direction of x axis |
| I | Current applied to the heater |
| k | Thermal conductivity |
| $k_{11}$ | Tensor component of thermal conductivity |
| $k_{33}$ | Tensor component of thermal conductivity |
| $l$ | the length of the tube |
| n | Number of thermocouples |
| q | Heat flux density |
| $\vec{q}$ | Heat flux vector |
| $Q_z$ | External heat flux |
| $Q_z^*$ | Resultant vector of heat flux |
| S | Sensitivity of the sensor |
| $S_0$ | Sensitivity of the Anisotropic thermoelement or Gradient Heat Flux Sensor |
| $S_{0max}$ | Maximum sensitivity of the sensor |
| $S_T$ | Seebeck coefficient of the materials |
| $T_1$ | Temperature of thermocouple |
| $T_2$ | Temperature of thermocouple |
| $T_W$ | Wall temperature |
| U | Voltage applied to the heater |
| aSoE | After Start of Energization |
| ADC | Analog-to-Digital converter |
| ATE | Anisotropic thermoelement |
| CFD | Computational Fluid Dynamics |
| CHT | Conjugate Heat Transfer |
| CPFR | Constant Pressure Flow Rig |
| CVHC | Constant Volume Hot Cell |
| CVPC | Constant Volume Pre-combustion Cell |
| DAQ | Data Acquisition |
| DC | Direct Current |

| | |
|---|---|
| DynPT | Dynamic Pressure and Temperature |
| GHFS | Gradient Heat Flux Sensors |
| HFS | Heat Flux Sensor |
| IMEP | Indicated Mean Effective Pressure |
| LFO | Light Fuel Oil |
| LIP | Light Induced Phosphor |
| LUT | Lappeenranta University |
| NPL | National Physical Laboratories in United Kingdom |
| ORE | Optical Research Engine |
| OSCC | Optical Spray Combustion Chamber |
| RCM | Rapid Compression Machines |
| RCYM | Rapid Cycling Machine |
| RTD | Resistance temperature detector |
| SoE | Start of Energization |
| TDC | Top Dead Center |
| TTL | Transistor-Transistor Logic |
| UK | United Kingdom |

# 1 Introduction

This thesis studied measurement of heat transfer within a combustion chamber. The focus was on heat transfer from spray combustion. Work was requested by Wärtsilä's Research and Technology Development department to provide reference data for simulation modules. The test rig used was the Optical Spray Combustion Chamber (OSCC) developed by Wärtsilä. This chamber can replicate conditions seen in combustion chambers of internal combustion engines. Similar test rigs have been built in different testing facilities for research purposes. The growing investment in and manufacturing of optical spray chambers is a direct consequence of new emission standards. Optimization methods for current engine designs exist, such as higher injection pressure, exhaust gas recirculation, and fine-tuning of injector nozzle geometry. Spray chambers are used to develop injector designs. The OSCC allows testing of injectors before installing them to engines. It also allows visual analysis of spray combustion to improve existing designs. New measurement techniques can also be used for further insight. This thesis investigated one of these techniques used for heat transfer measurement.

Measurement campaign also served as validation of the test rig for testing purposes. The OSCC can do both cold and hot injections inside the chamber. Testing was done in hot phase to measure heat transfer from the combustion spray. Measurement data would be used as a reference for the Computational Fluid Dynamics (CFD) modules. The OSCC provided the opportunity to design a simple simulation model for heat transfer analysis. Gradient Heat Flux Sensors (GHFS) were used to measure heat transfer from the spray combustion. These sensors were coupled to a component placed inside the combustion chamber. This thesis focused upon the heat flux measurements, preparation work and validation of the results. The goal was to validate the instrumentation method done on the sensors. The method needed to be capable of withstanding consecutive combustion sprays and to give accurate measurement data. Manufacturing and calibration of these sensors or CFD simulation work were not discussed. Evaluation methods of raw data were not included in this thesis. Other measurements done parallel during the tests were used for further analysis of the recorded heat transfer. These included high-speed video

recordings of the combustion spray and temperature measurements. The temperature measurements were also used to approximate heat flux on the instrumented component. Other measurement methods were not discussed in detail but mainly used as a supplement for heat transfer analysis. Measurement campaign was done with only one injector type and fuel amount to limit the scope of the measurement.

Literature work presented showed different testing platforms used to replicate the conditions seen in engine combustion chamber. Sapozhnikov et al. (2020) work on heat flux sensors was the reference for the heat flux measurement. GHFS created by the authors were utilized for this thesis. Professor Andrey Mityakov from LUT University collaborated with the calibration and manufacturing of the sensors. Other heat flux measurement technologies were shown in the literature work for comparison.

# 2 Literature review

The focus of this thesis was to measure with a sensor mounted to an object subjected to high heat transfer. The main method discussed is with Anisotropic thermoelement (ATE) also known as Gradient Heat Flux Sensor. Literature review also studied other methods used for heat flux estimation and test chambers with similar conditions to engine combustion chamber.

## 2.1 Optical spray chamber

The optical spray chamber allows optical measurements during spray combustion. Mostly used for visualizing diesel spray with a high-speed camera and for optimization applications. For example, measurements that require direct visual contact with the measurement area are also possible for example with a laser.

The minimal requirement to have a functioning test rig for diesel spray combustion is to replicate gas conditions inside a diesel engine. Implementation of the conditions varies according to the chosen optical spray combustion design. The Optical Research Engine (ORE) has the most similar gas conditions compared to engines. Optical windows installed on the piston and the liner allow visual contact to the combustion chamber. Indicated Mean Effective Pressure (IMEP) can reach up to 1.8 MPa on these types of test rigs. Baert et al. (2009) notes that main issues seen with ORE test rigs are spray penetration limits from piston bowl radius and shape, and flow field being complex from the turbulent environment. (Baert et.al 2009)

Another design possibility is the Rapid Compression Machines (RCM). The design has a piston that performs one compression stroke and is locked upon reaching Top Dead Center (TDC) position. The main difficulty seen with the RCM are high vibrations that limit the optical measurement techniques that can be used. The Rapid Cycling Machine (RCYM) has a piston design where combustion is done inside a cylindrical combustion chamber with optical access from several sides. Pressure and temperature levels

reproduced inside the RCYM are similar to diesel engines. However, the small volume of the chamber remains an issue. (Baert et.al 2009)

The Constant Pressure Flow Rig (CPFR) has a constant flow of pressurized gas inside a pipe where fuel is injected against the flow. Windows can be placed around the pipe in optimal positions for recording purposes. The CPFR is limited by the peak temperature and pressure levels, and time between measurements when changing temperature parameters. The Constant Volume Hot Cell (CVHC) is a test rig where a gas mixture is trapped inside an high pressure container and heated to a target temperature before diesel is injected to the cell. Gas composition control and chamber volume size on the CVHC are considered good. It is limited by its optical access and the peak pressure before injection. (Baert et.al 2009)

Pre-combustion method is used to increase the range of measurement conditions on the Constant Volume Pre-combustion Cell (CVPC). Lean fuel mixture is injected into the chamber and sparked for pre-combustion. Fuel from the injector is then injected into the chamber. The CVPC has the largest pressure and temperature range for injection conditions but is limited by its measurement interval and similarity with the engine gas conditions. (Baert et.al 2009)

## 2.2 Heat flux sensors

Methods to measure heat flux in an accurate manner especially in harsh environments are few when compared to temperature. In most cases measurement uses estimations done with the help of temperature sensors rather than using heat flux sensors. Temperature measurement sensors used are resistance temperature detectors (RTDs) or thermocouple sensors that are cheap and easy to use. Heat transfer coefficient correlations such as Taylor’s or Woschni’s use engine parameters and conditions to estimate heat transfer. Parameters include engine geometry, piston speed and gas temperature (Heywood, 2018).

Measuring conduction and convection to the wall would require either new heat transfer coefficient methods or heat flux sensors. There exist several types of methods and sensors to evaluate heat flux. General classification of these methods does not exist. Gerashchenko (1971) notes that there are optical and correlation methods, surface-mounted heat flux measurement methods and measurement of temperature difference through a known material. Surface-mounted heat flux sensors (HFS) are elements mounted on a foreign body that can measure heat flux through this body (Sapozhnikov et al. 2020). Advantages of HFS are low disturbance on the temperature field around the sensor, average local heat flux around the sensor area and a well-known method to measure DC voltage. Mounting position can have two different cases. The sensor placement is either inside or at the surface of the body. The Surface-mounted sensor's main characteristic is thermopower that is proportional to the external heat flux vector. For thermocouple–type or longitudinal–type HFS the generated thermopower $\overrightarrow{E_{||}}$ during transient state is collinear to the heat flux vector. Figure 1 shows a visual example of a generated thermopower collinear to the external heat flux vector.

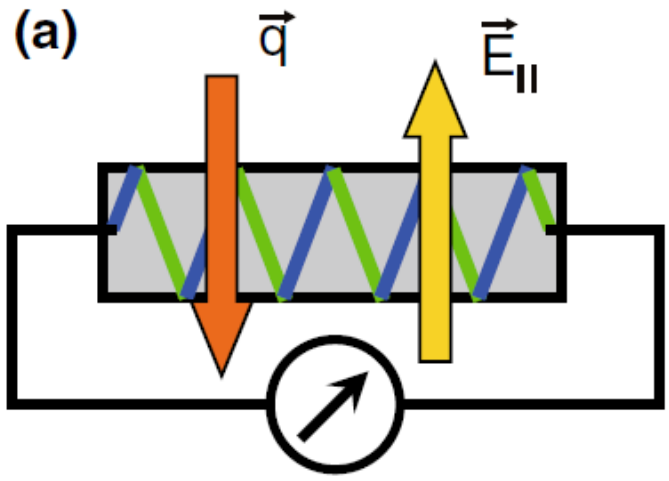


Figure 1. Heat flux sensor made of thermocouples and the generated thermopower from external heat flux vector (Sapozhnikov et al. 2020).

HFS has plates with differential thermocouple junctions mounted at the surfaces. Kutz (2013) details the theory and usage of longitudinal HFS elements. The measured voltage output E of the sensor is

$$E = nS_T(T_1 - T_2), \quad (1)$$

where n is the number of thermocouples, $S_T$ is the Seebeck coefficient of the materials (V/K), $T_1$ and $T_2$ are the different temperatures between thermocouples (K).

Thermoelectric sensitivity or Seebeck coefficient measures materials induced thermoelectric voltage from temperature difference across the material. Measured phenomenon in thermocouples is thermoelectric effect also known as Seebeck effect where electromotive force develops between hot and cold point (Kutz, 2013). Sensitivity of the sensor is

$$S = \frac{E}{q} = \frac{nS_T\delta}{k}, \quad (2)$$

where q is heat flux density (W/m$^2$), δ is thickness (m) and k is thermal conductivity (W/mK). When measured in steady–state mode, the temperature difference between the hot and cold junction points of the HFS are linearly proportional to the sensor plate thickness and electrical resistance. During transient state, the measured heat flux corresponds to

$$\vec{q} = -k\frac{\partial T}{\partial x}, \quad (3)$$

where x is the coordinate in the direction between cold and hot junction point and T is the temperature difference. X coordinate is collinear to the heat flux vector $\vec{q}$. For HFS the relation between the temperature and thickness causes nonlinearity for the sensitivity and thickness. Sapozhnikov et al. 2020 note that for longitudinal–type HFS this causes discrepancy between sensitivity and response time, which is fundamental and

irremovable. The advantage of modern HFS is its high volt-watt sensitivity, required size and response time. The limitation of HFS is its operating temperature range. For our tests inside the combustion chamber to measure spray combustion, the expected temperature range is in between 200 – 500 K. Different HFS response times and temperature ranges are presented in Figure 12 and Chapter 2.3.

One method mentioned to estimate heat flux is with measurement of temperature difference through a known material. Measurements made with thin-film thermocouples calculate the heat flux through the surface using hot and cold junction points. Thin film sensors mounted on the surface and to a known distance inside the body function as the measurement points. Figure 2 shows instrumentation design done by Li et al. (1997), where thermocouples measure the hot and cold junction points. To increase the accuracy on the local heat flux it is paramount to have the cold junction spot as perpendicular to the surface and as close to the same area where the hot junction spot is. The measured heat flux from these thin film thermocouples assumes that the local heat conduction is one-dimensional. This leads to inaccuracies in uneven surfaces and bodies where the material is not constant.

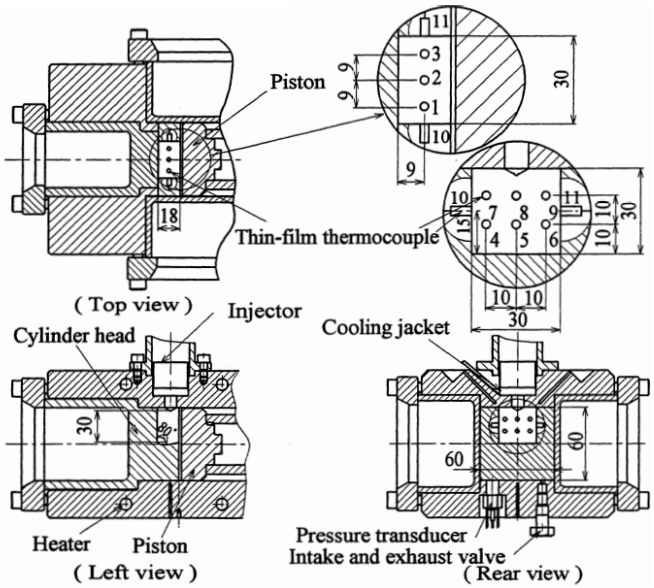


Figure 2. Combustion chamber and placement of thermocouples to measure heat flux (Li et al. 1997).

One method to limit this is to use cooling oil near the inner thermocouple position for constant temperature between the measurement points. This method also keeps the heat transfer perpendicular to the surface (Mahmud et al. 2019). If the body temperature in the cold junction point is colder than the surrounding area, the heat flow from the heating element will transfer in the assumed one-directional angle.

## 2.3 Gradient heat flux sensors

Other type of surface-mounted sensor has anisotropic thermal conductivity, electric conductivity, and thermoelectric coefficient. An electronic vector $\overrightarrow{E_{\perp}}$ generates along the anisotropic material when external heat flux vector $\vec{q}$ passes across it. Figure 3 displays this phenomenon. This thermoelectromotive force (thermo-EMF) is due to Seebeck's transverse effect. External heat flux vector produces transverse temperature difference along the anisotropic material (Anatichuk & Bulat, 2001). Temperature gradient exists along and across the material when applying external heat flux. Sapozhnikov et al. (1998) proposed that due to the heat flux being proportional to the temperature gradient these transverse type sensors should be called Gradient Heat Flux Sensors (GHFS).

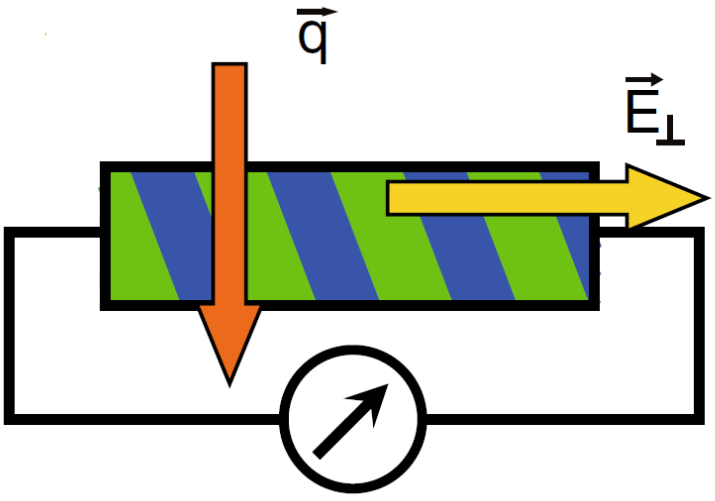


Figure 3. Heat flux across an anisotropic material (Sapozhnikov et al. 2020).

Electronic vector along the Anisotropic themoelement (ATE) can be measured by the following equation.

$$\overrightarrow{E_{\perp}} = -\hat{e} * \nabla T, \tag{4}$$

Where ê is Seebeck's coefficient (V/K) and ∇T is temperature gradient (K/m). Thermo-EMF $E_x$ (V) calculated is linearly related to the sensitivity of the ATE $S_0$ (Sapozhnikov et al. 2020).

$$S_0 = \frac{E_x}{Q_z A}, \tag{5}$$

Where $Q_z$ is external heat flux ($W/m_2$), and A ($m^2$) is the area of the Anisotropic thermo-element. Maximum sensitivity of anisotropic material $S_{0max}$ is with optimal cut angle $\theta_{opt}$ shown in Figure 4. Angle is dependent upon thermal conductivity tensor components that are according to the crystallographic axes $C_1$, $C_2$ and $C_3$ used in crystals (Sapozhnikov et al. 2020).

$$\theta_{opt} = \pm \tan^{-1} \sqrt{\frac{k_{11}}{k_{33}}}, \tag{6}$$

Where $k_{11}$ and $k_{33}$ tensor components of thermal conductivity.

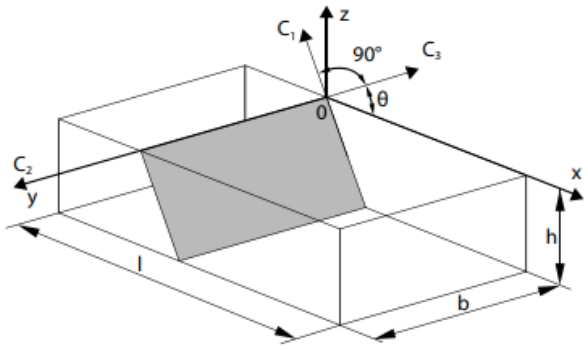


Figure 4. The anisotropic thermoelement. Coordinate axes x, y, z, dimension *l* x b x h and crystallographic axes $C_1$, $C_2$ and $C_3$ (Sapozhnikov et al. 2020).

Optimal cut required for the copper and nickel mixture displayed in Figure 5. Finished product after cutting produces alternating layers used for the Anisotropic thermoelement. Figure 6 displays an ATE made from copper and nickel after cutting procedure from Figure 5.

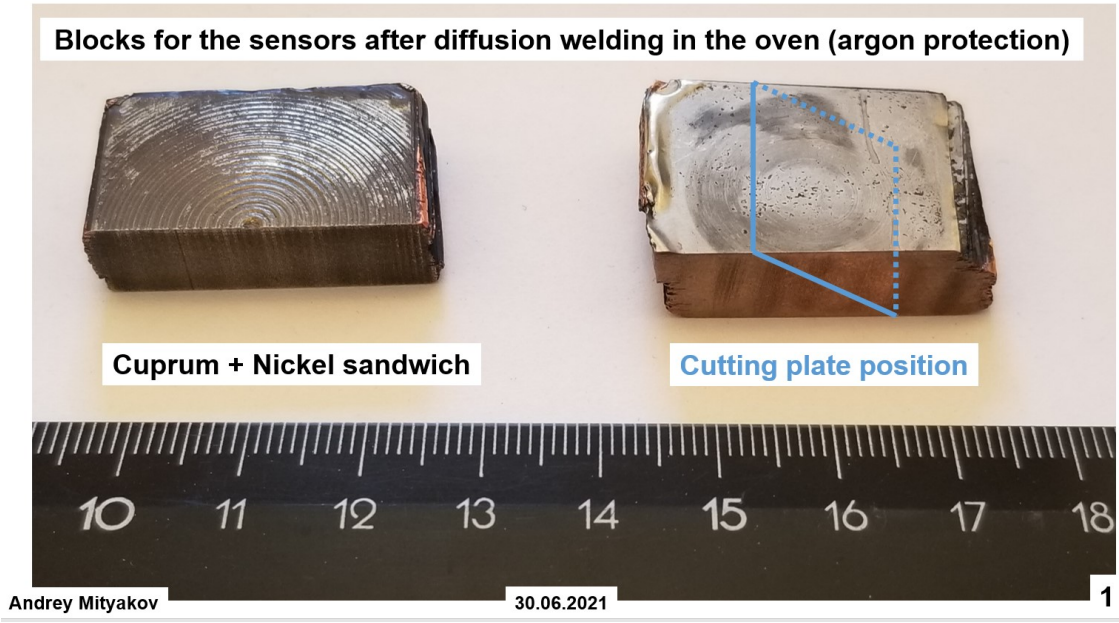


Figure 5. Mixture of copper and nickel before cutting procedure for GHFS production (Mityakov, 2021).

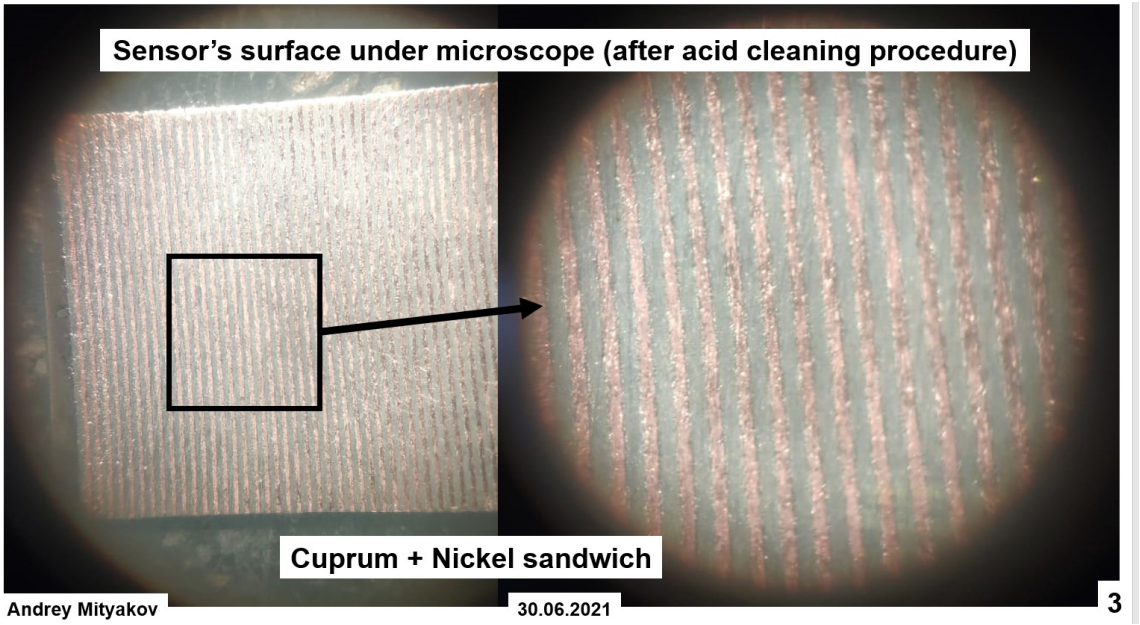


Figure 6. Anisotropic thermoelement when inspected with a microscope. Used GHFS mixture copper+nickel (Mityakov 2021).

Electric and heat flux vectors directional patterns shown in Figure 7. $Q_z^*$ is resultant vector of heat flux in ATE, $Q_z$ is external heat flux, $E_x$ is thermoelectric field strength in the direction of x axis and $\nabla T_z$ is Projection of temperature gradient onto z axis.

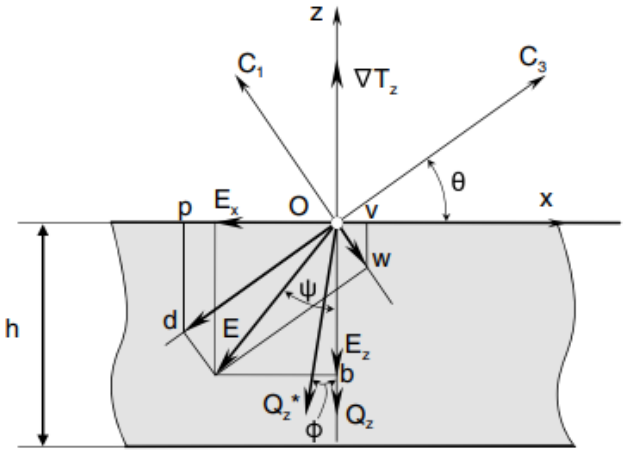


Figure 7 Electronic and heat flux vectors pattern in the ATE (Sapozhnikov et al. 2020).

Sensitivity measured is dependent on the width b of the Anisotropic thermoelement and the cutting angle used. Figure 8 shows an example of this with bismuth based ATE. The mean thermodynamic temperature of the given medium affects thermal conductivity, which causes sensitivity change. Different compositions have shown different sensitivity curves. Figure 9 shows sensitivity curves of two compositions.

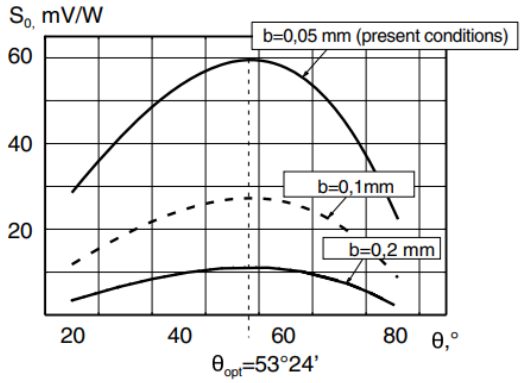


Figure 8. Sensitivity graph of bismuth based ATE with different widths and cut angles (Sapozhnikov et al. 2020).

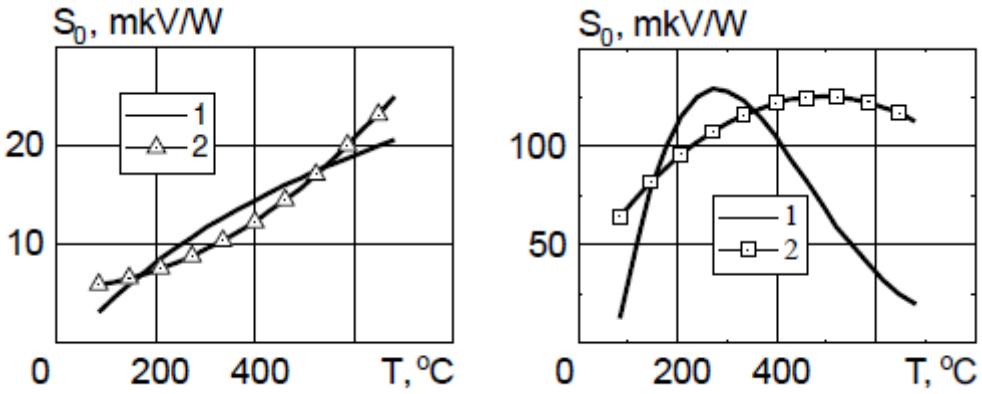


Figure 9. The calculated and measured sensitivity curves of two compositions. Curve numbers correspond to 1 - calculated and 2 - measured. The left graph represents chromel + alumel and the right graph nickel + stainless steel (Sapozhnikov et al. 2020).

Sapozhnikov et al. (2020) have measured sensitivity of different compositions and working temperature limits presented in Table 1.

Table 1. GHFS's Volt-Watt sensitivity at 300K (Sapozhnikov et al. 2020).

| Composition | Average sensitivity (mV/W) | Working temperature (◦C) |
|---|---|---|
| nickel + stainless steel | 0.40...0.8 | 1400 |
| chromel + alumel | 0.35 | 1200 |
| titan + molybdenum | 0.02 | 1660 |
| Nichrome + steel | 0.5 | 1100 |
| Copper + constantan | 0.2 | 1000 |
| chromel + alumel | 0.1 | 1450 |
| silicon + aluminium | 1.0 | 700 |
| p-silicon + n-silicon | 1.5 | 800 |

Calibration of GHFS requires a known heat source. (Sapozhnikov et al. 2020) provides schematics used for calibration of GHFS in Figure 10. An electric heater produces heat transfer to the sensor mounted to a base. Thermal insulation applied around the module limits heat losses to the environment. Setup accuracy is between 0.2 – 1 % with low heat flux but increases to 6 – 8 % when reaching 600 – 1000 kW/m$^2$. Inaccuracy in high temperatures is caused by heat losses from radiation and convection.

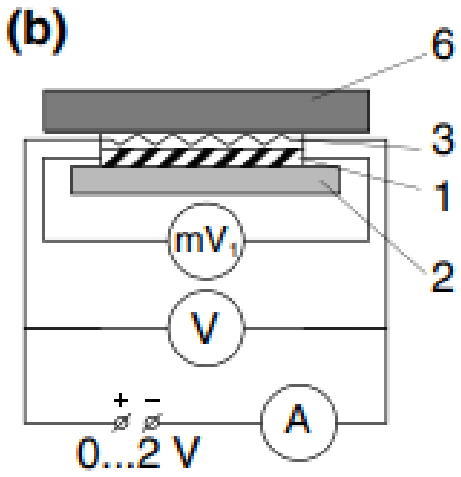


Figure 10. Calibration setup for GHFS. Labels correspond to 1: Calibrated GHFS, 2: the base, 3: the heater and 6: the thermal insulation. User controls the heat transfer produced from the heater (Sapozhnikov et al. 2020).

For higher temperatures Sapozhnikov et al. (2020) designed an isolated setup to reduce heat losses. Figure 11 shows the improved design that places the sensor inside a vacuumed space. Convective heat loss is removed by the vacuumed space inside the cylindrical body. Heat radiation is transferred from the heater to the nickel foil tube where GHFS is mounted. Nickel foil has low thermal resistance that limits losses from the conductive heat loss. With this setup the majority of the heat radiating from the heater is transferred through the cylindrical tube. Sensitivity $S_0$ is calculated from output power of the heater and measured voltage.

$$S_0 = \frac{E*\pi*d*l}{U*I*A}, \quad (7)$$

Where E is voltage from the sensor, d is diameter of the nickel foil tube, $l$ is the length of the tube, U is voltage applied to the heater, I is the current applied to the heater and A is the area of the sensor (Sapozhnikov et al. 2020).

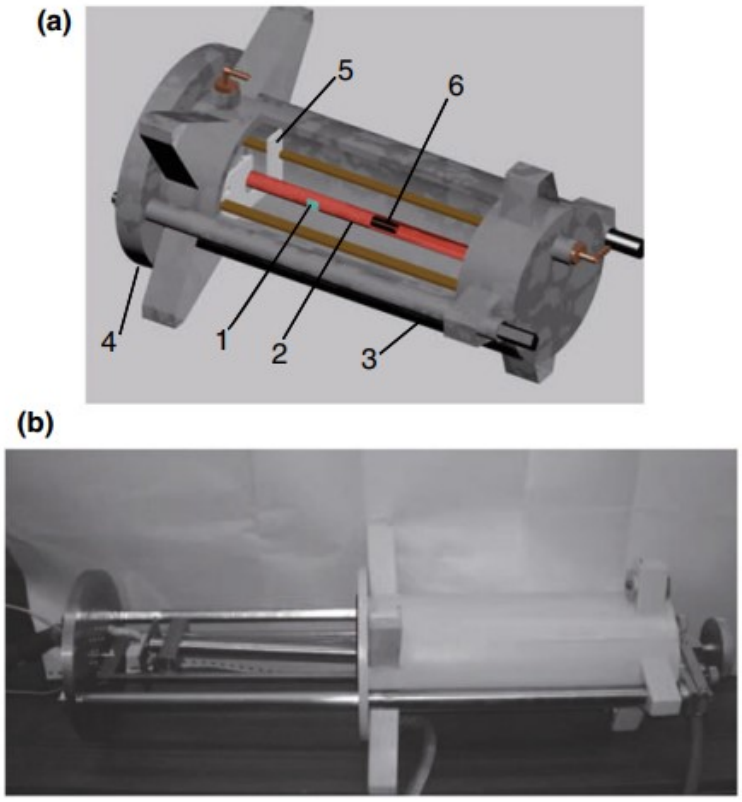


Figure 11. Point of interest (a) design (b) of high-temperature calibration of GHFS. 1: the calibrated GHFS, 2: the tube, 3: the body, 4: the cover, 5: the holder, 6: the thermocouple (Sapozhnikov et al. 2020).

GHFS have high response time ranging between $10^{-8}$ and $10^{-9}$ s and are capable of withstanding high temperatures. Depending on the used material it can have working temperatures reaching 1400 K. Limitation for the GHFS is in its low volt-watt sensitivity when compared to HFS. Figure 12 shows the response time and sensitivity of the modern HFS and GHFS. For our purpose with mounting heat flux sensors inside the hot combustion chamber high temperature resistance is seen as positive. Low sensitivity does not limit the measurement due to high heat flux expected from the spray combustion.

In most cases the sensor material differs from the mounted body which causes disturbance in the temperature field. Difference in thermal resistance leads to different thermal values compared to the surrounding surface (Van der Graaf 1990). By Mityakov's (2021) estimations this thermal resistance causes 5% error on the copper + nickel GHFS and stainless-steel + copper used in our measurements.

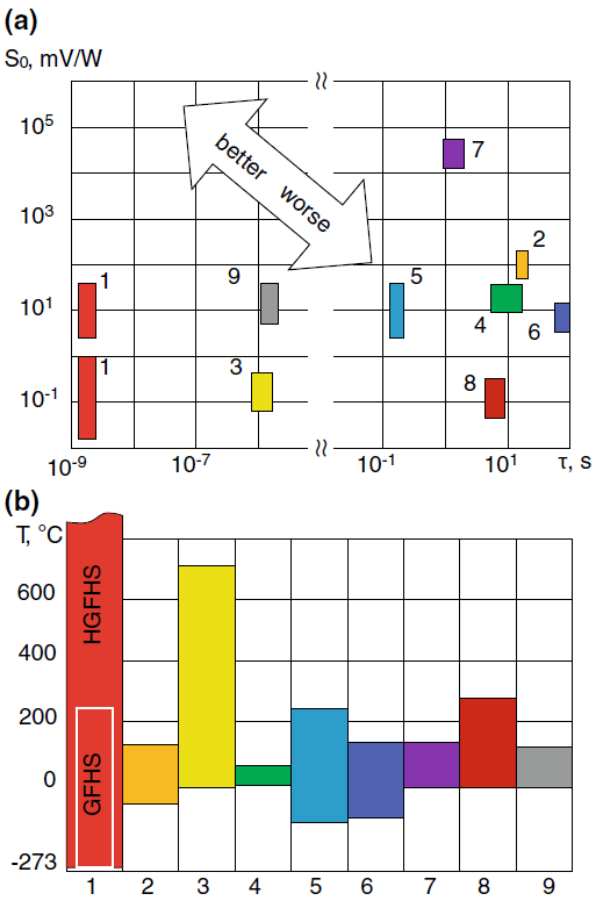


**Fig. 1.11** Comparison of modern heat flux sensors by sensitivity $S_0$ and response time $\tau_{min}$ (**a**) and temperature limit (**b**): 1—GHFS based on bismuth (**a**) and HGHFS (**b**); 2—Academy of Science, Ukraine; 3—Vatell (USA); 4—Wuntronic (Germany); 5—Captec (France); 6—Hukseflux (Netherlands); 7—Physical Electronics Laboratory (Switzerland); 8—Newport (USA); 9—TNO (Netherlands); 10—ALTP from FORTECH HTS GmbH (Germany) (no data on a working temperature)

Figure 12 Modern heat flux sensors' sensitivity and response time (Sapozhnikov et al. 2020).

# 3 Methods and measurement

## 3.1 Optical spray combustion chamber

Test rig used during these measurements was an Optical Spray Chamber (OSCC) that was in its final building phase for hot stage testing. This stage allowed controlled spray combustions inside the chamber. There are several distinctive designs for optical test rigs that function differently and have different benefits and drawbacks that were discussed in Chapter 2.1. Test rig used is a Constant Volume Pre-combustion Cell (CVPC) with a Constant Volume Hot Cell principle (CHVC). Internally Wärtsilä calls this test rig Optical Spray Combustion Chamber (OSCC).

Figure 13 shows general information of the OSCC. The chamber is large in design, allowing medium and large bore engine injectors testing inside the chamber. OSCC has a constant volume inside the chamber with four optical window sides. All sides are replaceable with dummy modules. The used injector is installed to the bottom injector module. Mixed gas ignited by a spark plug controls the pressure inside the chamber. Result of this gas combustion is a gas mixture that replicates conditions in an engine combustion chamber. Following the combustion pressure slowly decreases to target pressure where the injector sprays fuel to the chamber. Fuel spray ignites due to the conditions inside the chamber. To differentiate between the two combustions, the combustion caused by the spark plug is called pre-combustion and the burning of the injection spray as spray combustion. Whole sequence is called the combustion sequence.

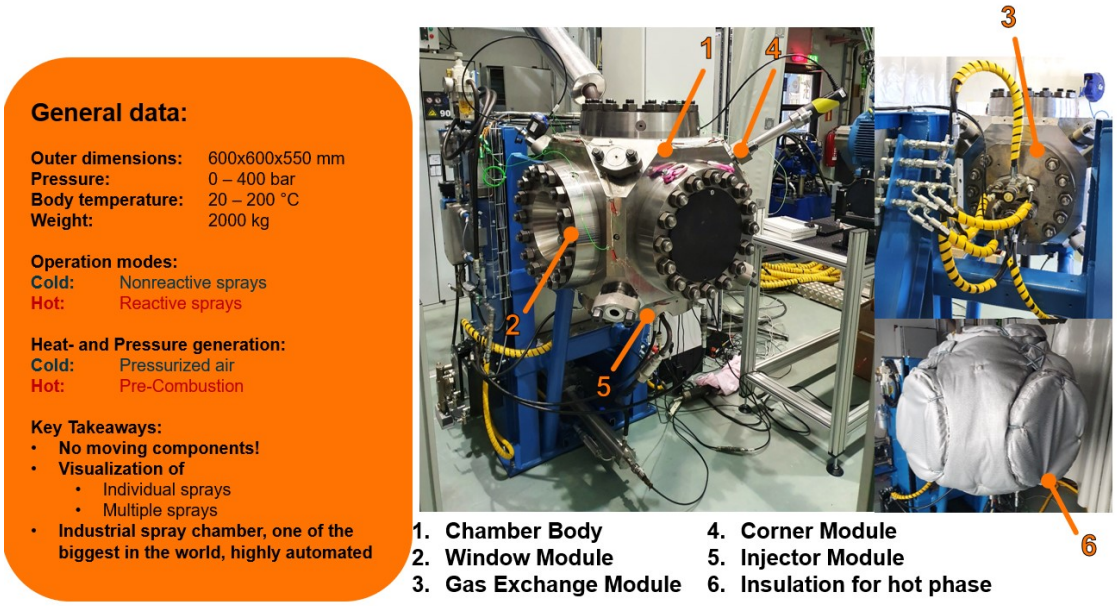


Figure 13. The Optical Spray Combustion Chamber (OSCC) where the measurement campaign was done.

Before the pre-combustion gas fills inside the chamber for ignition. Figure 14 shows an example of how the pressure increases. Before adding the gases, the chamber is fully vacuumed to remove external gases. This sequence shows any leakages due to failing the vacuum check. Depending on the target pressure and current temperature the gas mixture contains a specific amount of fuel gases, nitrogen, and oxygen. Filling order is fuel gases, the inert gases and anything containing oxygen. Mixing time is added after the gas fill sequence to allow mixing before ignition. Spark plug placed inside the chamber initiates the ignition of the gas mixture. Figure 14 shows the pre-combustion pressure curve where target pressure was 60 bars.

For our measurements pre-combustion and gas filling causes most issues for a successful GHFS installation. Gas filling sequence requires a vacuumed chamber beforehand. Instrumented components with GHFS cannot cause any leakages when installed to the OSCC. Cable routes would be required to be sealed in the case of the adhesive layer breaking. Another problem noticed was pre-combustion pressure rise rate with rich air-fuel ratio. With a rich air-fuel ratio chamber pressure signal started to fluctuate. This phenomenon seen in Figure 15 is comparable to knocking seen in engines. Exposure to high pressure rise rate can shorten the lifespan of pressure sensors. This can cause issues

with instrumented GHFS. Adhesive layer especially being a critical weak point that can break from high pressure rise rate**.** It might be that any added instrumented GHFS would not be able to manage consecutive pre-combustion sequences. Thus, testing required a lean air-fuel ratio for pre-combustion.

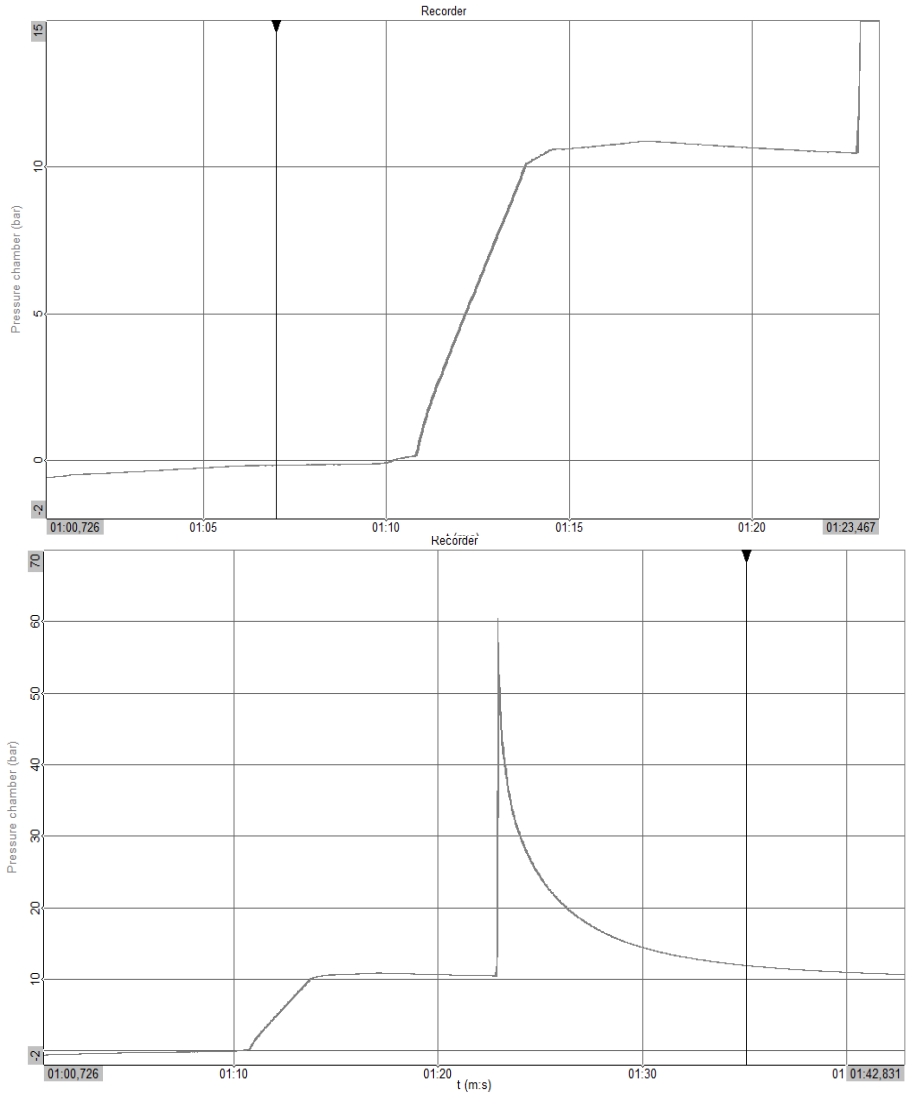


Figure 14. Pressure curves during pre-combustion. In the upper image it shows the mixing of gases, and in the lower image shows the entire sequence with peak pressure.

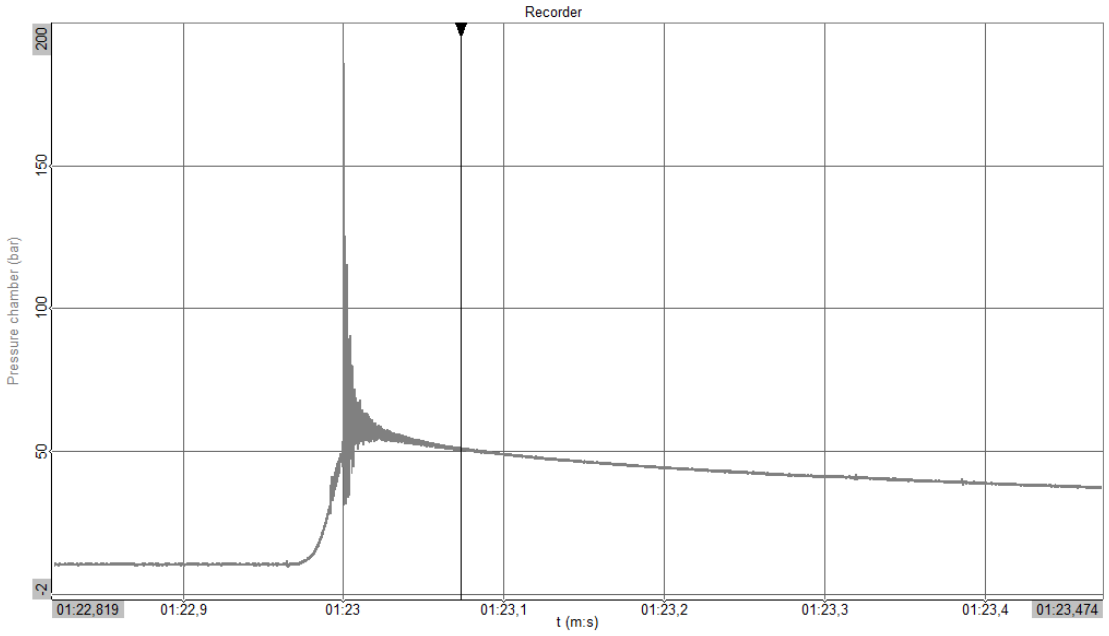


Figure 15. Raw signal of pressure signal inside the OSCC. Showing a similar phenomenon as knocking inside engines.

## 3.2 Chosen gradient heat flux sensor

Andrey Mityakov (2021b) provided chosen Gradient Heat flux Sensors (GHFS) for testing purposes. Chosen shape for the sensor was a square with the soldering joints for the sensor wires placed to corners. Two batches of sensors were received to be mounted on the instrumented components. Size of the sensors were 15x15 and 10x10 mm for the corner module and the instrumented plate. The larger ones were made from stainless steel + copper and the smaller ones from copper + nickel. In both cases sensor thickness was 0.5mm. Initial tests used the larger sensors to have a stronger voltage signal. The measurement campaign used the smaller sensors to fit more sensors to the instrumented component. For electric insulation of the wires used Teflon tube material. Two possibilities for the wire material were chrome nickel alloy and copper. For our purposes using copper was easier. To extend sensor wire copper wire was used. Figure 16 shows both sensor types. Wires were attached to the sensor by laser soldering. Soldering joint

was a critical point for breaking and could not manage much bending. Heat transfer sensitivity of the GHFS was 1mV/W where heat flux sensitivity was determined by the size of the sensor.

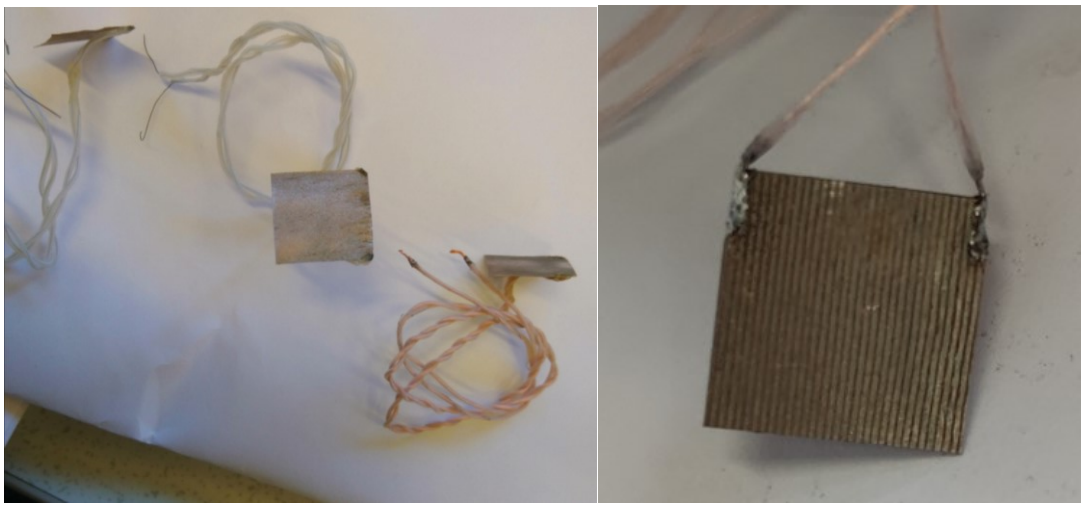

Figure 16. Stainless steel + nickel sensors of 15x15 mm (left) and 10x10 mm copper + nickel (right).

## 3.3 Component instrumentation preparation work

Goal of the instrumented corner module was to find a new optimal design for a sensor plug to measure inside the OSCC. It would give data on the measured heat flux and on the durability of the instrumentation design. Improved instrumentation would be then done to the instrumented plate. Previous results with a sensor plug shown in Chapter 3.3.1 were used as a basis for what requirements were focused upon (Riiki, 2014). The expertise of Tomi Riiki and Andrey Mityakov (2021) were used to help with the planning of instrumenting the sensors to the modules and the measurement plate. For example, how thick the adhesive layer should be for accurate results while the GHFS would stay mounted. Discussions included the cable route design and how to avoid breaking the soldering joint when placing the sensor. Modified corner module design followed these key points. Design of the modified corner module was by Viljam Grahn (2021) who was co-operating his own thesis at the time on surface temperature measurement techniques on optical spray chambers and the main designer of the OSCC. Furthermore, the

design for the measurement plate and the planning of the cable routing through the combustion chamber was by Grahn (2021).

### 3.3.1 Previous GHFS designs for engine testing in Wärtsilä

The main discovery from the previous tests done with GHFS in Wärtsilä was the requirement of a robust adhesive layer for the sensor (Riiki, 2014). The high-pressure environment especially caused cracks to appear in the solid adhesive. Figure 17 shows the glued sensor before and after measurement. Soldering joints for the were on the side of the sensor and would go through the plug from a cable feedthrough. Ceramic glue would hold the sensor in place and to remove any leakages. Conclusion made from how the ceramic glue broke was that excess adhesive surrounding the sensor was detrimental. Exposure to the combustion conditions for the adhesive layer should be minimal. Due to ceramic glue failing alternative adhesive solutions were tested.

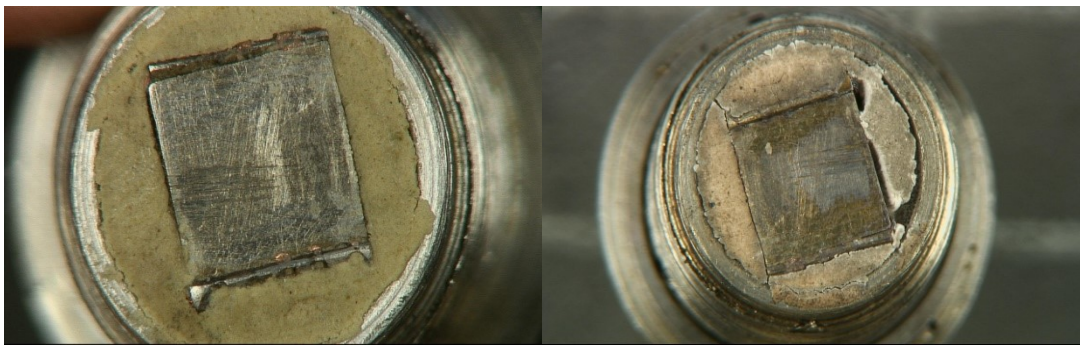

Figure 17. Plug sensor that was installed inside the engine. Before and after testing. (Wärtsilä 2014)

### 3.3.2 Adhesive testing with corner modules

Five different adhesives were evaluated to find the best alternative. Requirement for usable adhesive was that it was able handle high pressure and temperature conditions. Adhesive also needed to be able to bond two metals and be an electrically insulating material. The OSCC was not in use for combustion testing with the adhesives. It was possible to raise pressure up to 100 bar for the adhesive testing. Temperature testing

was done inside an oven in 195 °C. Chosen adhesives were commonly used in other instrumentation works in Wärtsilä. These include gluing strain gauges, thermocouples, and telemetries in harsh environments around and inside the engine. Table 2 lists tested adhesives. These adhesives were either epoxy based, or structural acrylic based.

Table 2. List of used adhesives in dummy corner modules to choose for instrumentation (Henkel 2022, HBM 2022 & Kyowa 2022).

| **Adhesive** | **Type** |
|---|---|
| Mega Cryl SST NCH | Structural acrylic |
| EA 9492 Loctite | Epoxy |
| Mega Stack NCH | Structural acrylic |
| X280 HBM | Epoxy |
| EP-34B Kyowa | Epoxy |

Dummy corner modules were glued with a 1 mm thick stainless steel 20 $mm^2$ square plate that represented the sensor. Copper wires were soldered on the sides of the sensors to assess the cable route design. The electrical insulation of the adhesive was also tested. If the insulation would fail it would cause noise and minimize the signal strength due to ground loop effect. Sensors would also have to be recalibrated.

Electrical insulation for the wires was measured from the electrical resistance with a multimeter before, during, and after heating and pressure tests. The insulation worked if the values stayed the same. During tests visual cracking or durability loss on the adhesive was monitored. Figure 18 shows corner modules in the oven after 1 hour. No visual cracking seen in any of the adhesives used. Only the surface of the glue changed to yellowish or brownish due to heat radiation and convection. All adhesives were also able to pass the pressure test. No issues seen with electrical insulation. From these results the decision was that testing would continue with combustion testing.

Figure 18. Two dummy corner modules with two different adhesives.

### 3.3.3 Corner module and instrumented plate design

The corner module design was modified to fit the GHFS. Appendix 1 shows drawing made for the modified corner module with cable routing for the heat flux sensor. The corner module was cut in half for a soldering port connection. The sensor placement was on the sensor pit placed on the surface of the corner module. Groves made for the sensor wires went from the cable feedthrough to two corners. Sharp edges around the cable feedthrough were rounded to remove damage to wires from the grinding burr. Size of the hole depended upon the insulated sensor wires. Figure 19 shows the details of the cable feedthrough and machining done for the sensor pit. Chosen thickness for the GHFS was 0.5 mm, which meant that the rest of the depth was for the adhesive layer. Mityakov (2021) noted that for accurate results from the measurements the adhesive layer needs to be as thin as possible. Minimum thickness for the adhesive used was 0.1mm for good mounting (Tomi Riiki 2021). In total the sensor pit depth was 0.6 mm. The depth accounted for the sensor thickness and the adhesive layer. The sensor pit area was 15 $mm^2$ to limit the adhesive exposed to combustion.

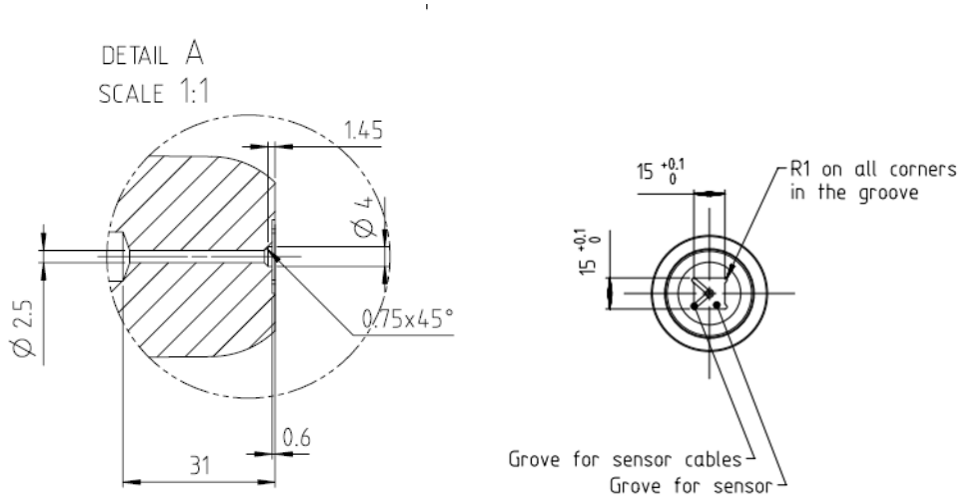


Figure 19. Point of interest from the modified corner module design. Cable feedthrough thickness and round edges chosen with the wires in mind.

The instrumented measurement plate was designed for the measurement campaign done with spray combustion. The goal was to design a plate with sensors that would be placed in an angle where an injector nozzle would spray fuel that would combust directly to the plate. Main concerns were how to instrument GHFS to the plate, how to get wires out of the chamber without causing any pressure leakages to the chamber, and how long these sensors would be able function in this hazardous environment. If the instrumentation would fail, any leakages would put measurements on hold without properly sealing cable routes.

Sensor placement was done according to the center point of contact from the spray combustion. One sensor was at the assumed center point of the spray combustion. Three sensors were placed 15 mm away from the center. Fifth sensor was placed 30 mm away from the center point of the spray combustion. This would allow measuring the heat transfer from the spray combustion to the plate depending on the distance from the

center point. If placed correctly, the center sensor would measure the highest heat flux. Other sensors would measure lower values depending on the distance away from the center. To allow several GHFS to be placed on the measurement plate it was decided that sensor size would be reduced to 10x10 $mm^2$. Changes were done to the sensor pit accordingly but were otherwise similar to the corner module design. An example sensor can be seen in Figure 20.

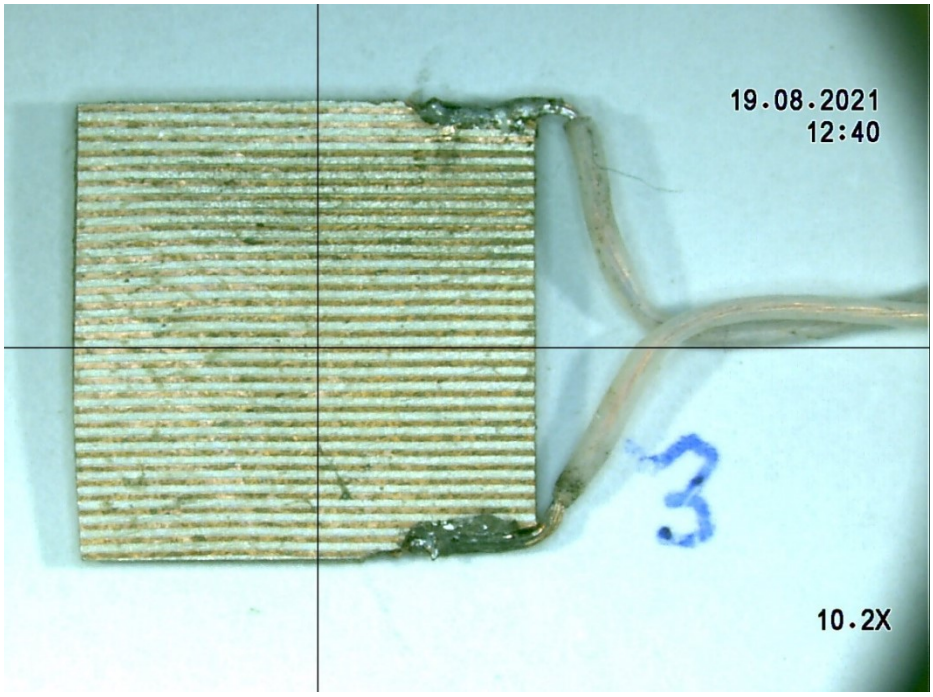


Figure 20. Gradient Heat Flux Sensor 3, the same as in the center position of the measurement plate.

Designed measurement plate can be seen in Figure 21. Design required two cable feedthroughs for all the sensors. Minimal amount of cable feedthrough was preferred to limit leakage spots. Four sensors would be installed to the same vertical line using the same cable route to the soldering terminal. These sensors would be named GHFS #1 – 4 from bottom to top with the center sensor being GHFS #3. Another hole would have to be machined for the sensor horizontally parallel to the center sensor. This sensor would be called GHFS #5. Table 3 shows sensor names with description where these sensors were placed on the measurement and sensitivity. These sensor positions are also numbered

in Figure 21. Connection between the cable feedthrough and sensor pit would be performed with a 45-degree angle drill hole to limit strain caused to the sensor wires by the edge between connecting drill holes. Due to the placement of the instrumented plate, the soldering terminal was installed inside the cable route. The wires soldered to the soldering terminal would continue outside of the OSCC through cable channels. These cable channels are sealed outside of the pressurized Optical Spray Combustion Chamber with an O-ring around the soldering terminal position. The O-ring placement is shown in Figure 21 with dark blue color. Appendix 2 shows drawings made for the instrumented plate.

Table 3. Sensor position, size, and sensitivity. Copper + nickel GHFSs were used for the instrumented plate.

| Sensor | Position from the center of the spray (mm) | Sensor size ($m^2$) | Sensitivity mV*W |
|---|---|---|---|
| GHFS #1 | 30 mm (bottom) | $9.025*10^{-6}$ $m^2$ | 1 $mV/m^2$ |
| GHFS #2 | 15 mm (bottom) | $9.025*10^{-6}$ $m^2$ | 1 $mV/m^2$ |
| GHFS #3 | 0 (center) | $9.025*10^{-6}$ $m^2$ | 1 $mV/m^2$ |
| GHFS #4 | 15 mm (top) | $9.168*10^{-6}$ $m^2$ | 1 $mV/m^2$ |
| GHFS #5 | 15 mm (right) | $9.111*10^{-6}$ $m^2$ | 1 $mV/m^2$ |

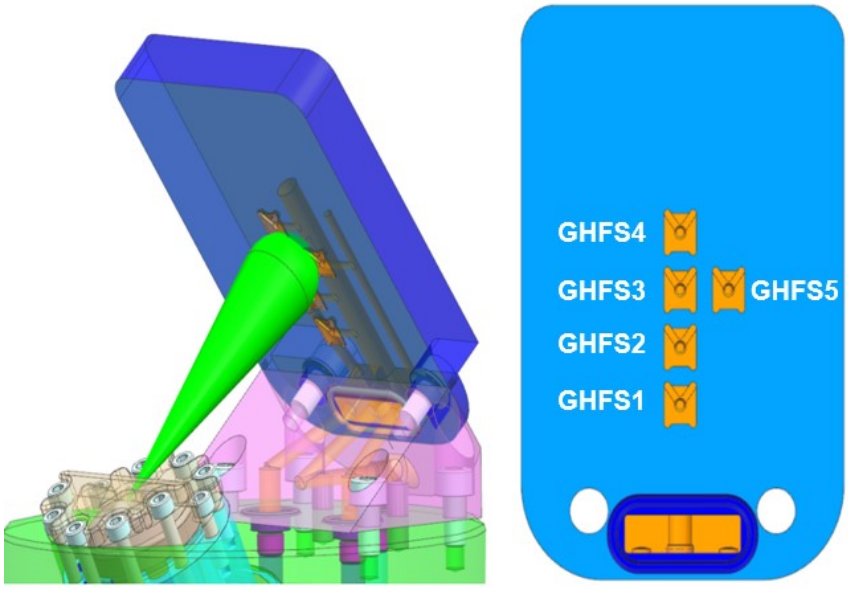


Figure 21. Placement of sensors and the spray target on the instrumented plate design.

### 3.3.4 Corner module and instrumented plate sensor installation

Instrumentation of the corner module started without founding a suitable alternative for the adhesive. Initial results showed no marginal difference between the adhesives. Chosen product was MegaCryl SST widely used in other instrumentation. Same adhesive was in use in all other gluing procedures thereafter. Initially the plan was to assess all adhesives' durability to combustion sequence. Time delays in the validation of the OSCC hot stage made it not possible to assess adhesives before gluing the sensor to the corner module or the instrumented plate.

Modifications were made to the corner module before starting the instrumentation. The crucial issues from the initial design were the cable routes for wires and the soldering joint corners. The current design for the cable routes needed expansion to fit the sensor wires. The soldering joints also did not have enough space in the sensor pit and needed a larger machined area to fit. Expansions made to the original square shaped sensor pit was due to the GHFS. The sensors were made by hand that caused marginal errors on the size and made them rhomb shaped. Figure 22 shows the modified sensor pit. The modifications were kept small to minimize any effect on the heat flux measurements.

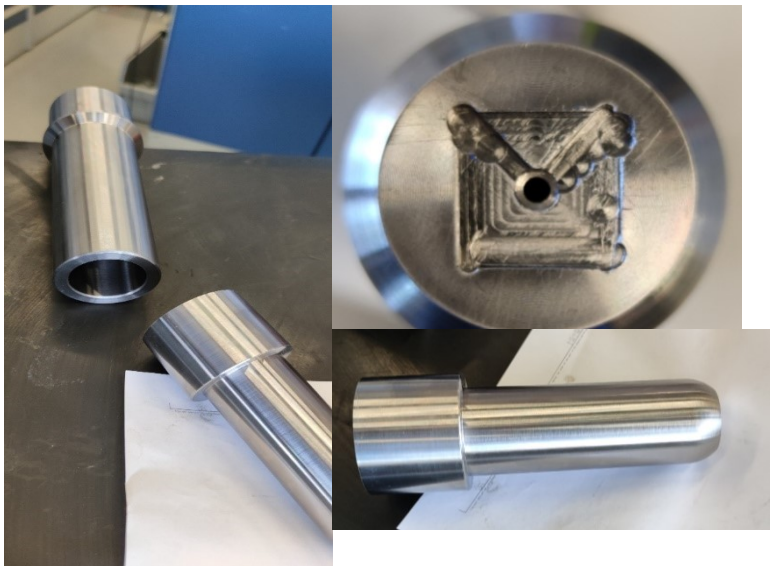

Figure 22. Pictures of the modified corner module.

Placing of the sensor to the sensor pit had the highest chance of breaking the sensor. Due to the thickness of the sensor, it was easily bendable with any applied force. This

could cause cracks on the sensor or to break the soldering joint connection. If either of these happened sensors would require recalibration and resoldering. Figure 23 shows a sensor that had its wiring resoldered with standard soldering tools.

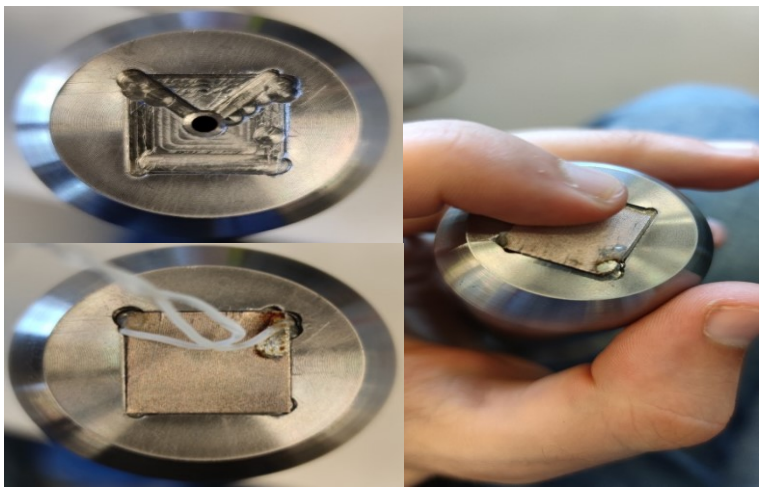

Figure 23. Fitting of a Gradient Heat flux Sensor. The bottom left picture shows that the right-side wire was soldered without the use of laser soldering.

Due to previously stated issues mounting was done carefully before gluing. Figure 24 shows stages of the instrumentation procedure. Gluing process started by applying the adhesive to the cable feedthrough hole to seal it. Then an excessive amount of adhesive was applied to the sensor pit. Excess glue would ensure no air bubbles would form to the adhesive layer. Any surplus glue was removed before placing a weight on top of the sensor. As seen in Figure 24 a magnetic weight was placed to hold the sensor in place until the adhesive would solidify. Layer of Teflon sheet was between the magnet and the sensor to not glue them with each other. The right most pictures from Figure 24 shows excess glue after removing the weight. The greenish color glue caused concern of failed adhesive hardening. Closer inspection showed that the greenish fluid was only on the surface of the GHFS. During the gluing process, any adhesive between the sensor and Teflon did not have the intended chemical reaction. The adhesive layer under the sensor solidified successfully. Green glue was cleaned from the sensor.

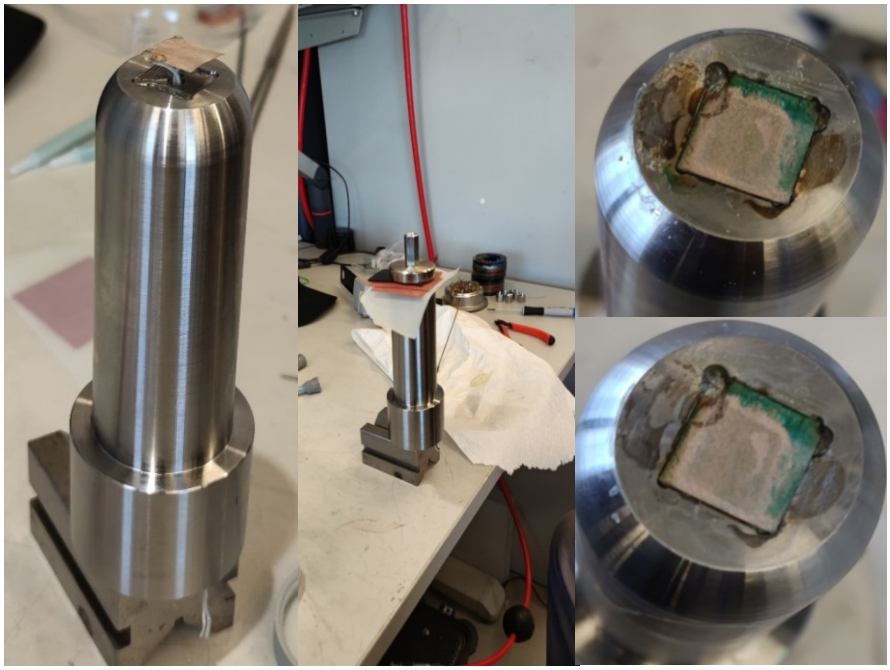

Figure 24. Gluing the Gradient Heat flux sensor to the corner module. The adhesive used was Mega Cryl SST.

The measurement plate required similar machining changes done to the sensor pit as with the corner module. Sensor instrumentation was prepared similarly with four sensors at the same time due to the placements of the cable routes. When placing the sensors extra care was focused upon not bending the wires too many times. The soldering joints are quite brittle and could handle bending of sensor wires to one side 2 – 3 times. Due to concerns of ground loop, pieces of Teflon sheets were placed under the sensors during the gluing process. The goal was to limit chances of the sensor directly touching the metal. After adhesive layers solidified, the cable feedthroughs were sealed with electrically insulative epoxy. Epoxy was used due to concerns of leaking caused by failed instrumentation. Specifically adhesive layer breaking due to exposure to combustion. As the measurement was done in parallel with other measurements the instrumentation had to be robust enough to not hinder the measurement campaign. Figure 25 shows preparation done to the instrumented plate. Epoxy used is still liquid in the right picture.

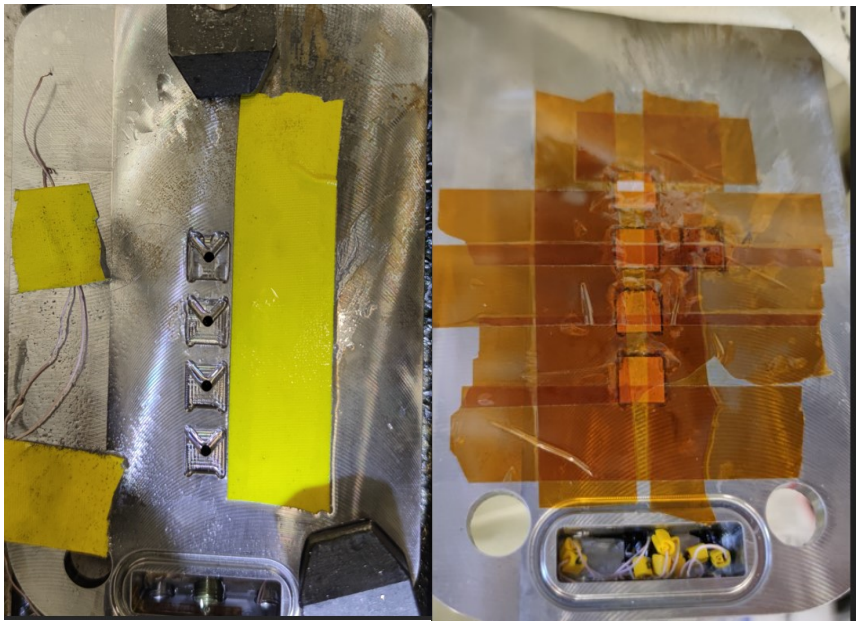

Figure 25. Instrumented plate preparation.

### 3.3.5 Sensor wiring for the corner module and the instrumented plate

The soldering terminal was placed to the backend of the corner module as a strain relief and connection point. The measurement used soldering terminals commonly in use with strain gauges. The chosen terminals were copper and nickel–plated soldering terminals manufactured by HBM (2022). The terminals have a polyimide plastic base with the plating mounted on top. The soldering terminal used was Model LS4 by HBM. The maximum operating temperature for the soldering terminal was 180 °C and briefly up to 260 °C. The measurement campaign will have the OSCC heated to 100 °C before pre-combustion. The likelihood of the soldering terminal reaching maximum operating temperature was minimal. The soldering iron chosen was also lead-free to have a higher operating temperature. The soldering terminal was glued using the standard guideline provided by HBM (2022a). The soldering terminal was prepared on a porcelain tile cleaned from dust, lipids, rust, and other particles with a solvent mixture. A polyimide tape was placed on top of the soldering terminal to install it to the corner module. Figure 26 shows the soldering terminal on the porcelain tile during this process.

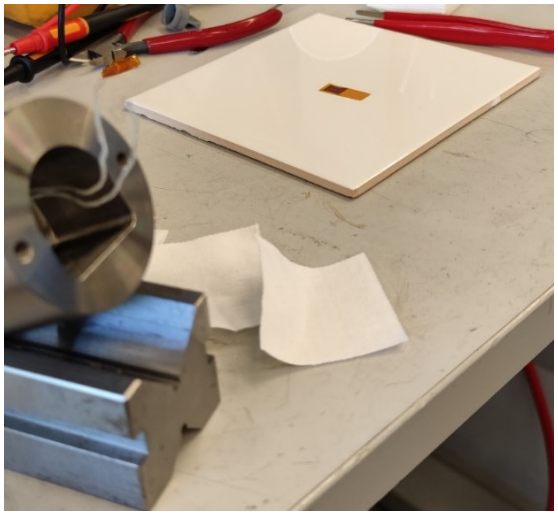

Figure 26. Soldering terminal on the porcelain tile. Polyimide tape placed on top of the terminal with excess tape for flipping. Corner module with sensor wires ready for soldering.

The corner module preparation required cleaning the surface for the soldering terminal. Any contaminants on the surface or on the soldering terminal would ruin the bonding between them. To help with the bonding process the surface on the corner module was roughened with an abrasive paper. Uneven surfaces improved the bonding for the adhesive layer. The adhesive used was Kyowa CC-33A (Kyowa 2022). Figure 27 shows when the adhesive was applied on the corner module surface. The soldering terminal was placed on top of the adhesive layer. The polyimide tape was grabbed with tweezers to avoid contaminations. To help with the bonding process minimal pressure was applied on top of the terminal for 15 to 60 seconds.

Figure 27. Soldering terminal glued to the corner module dummy. After applying the adhesive, the terminal was placed on the spot with tweezers.

After the soldering terminal bonded with the corner module, the sensor wires and the connection wires were soldered to the soldering pads. Fast soldering was preferred, which meant that soldering tips with high heat capacity should be chosen. Chisel-based or rounded tips were optimal while spiked tips would have too low heat capacity (HBM 2022). Soldering iron temperature was at 345 °C and soldering time was at minimum to limit exposure to heating. In the worst case the soldering pad on the terminal would loosen due to excess heat. The soldering pad and wires were pre-tinned to accelerate the soldering procedure. The soldered wires were glued to the corner module. The adhesive would function as an additional cable strain relief between the terminal and the sensor.

Figure 28 shows the corner module with the wires soldered and glued to the surface. The connection wires were 0.3 mm diameter copper wires. Initially the wires were 0.5 mm thick. Due to the weight of the copper wire, the glued soldering terminal detached from the corner module.

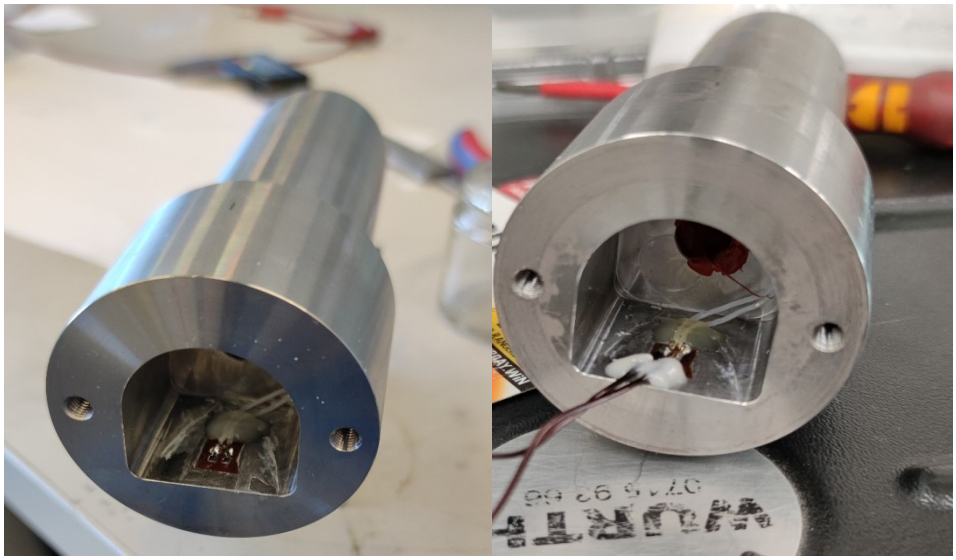

Figure 28. The soldering terminal with wires soldered. Adhesive added on both sides to limit strain to the terminal.

The LS4 Soldering terminal was also used for the instrumented plate. The soldering terminal required ten soldering pads to fit all sensor wires for soldering. Figure 29 shows the wiring work done to the instrumented plate. Preparation work was the same as with the instrumented corner module with additional adhesive used to hold wires in place.

The connection wires went outside of the OSCC along the cable routes and were connected to the measurement device.

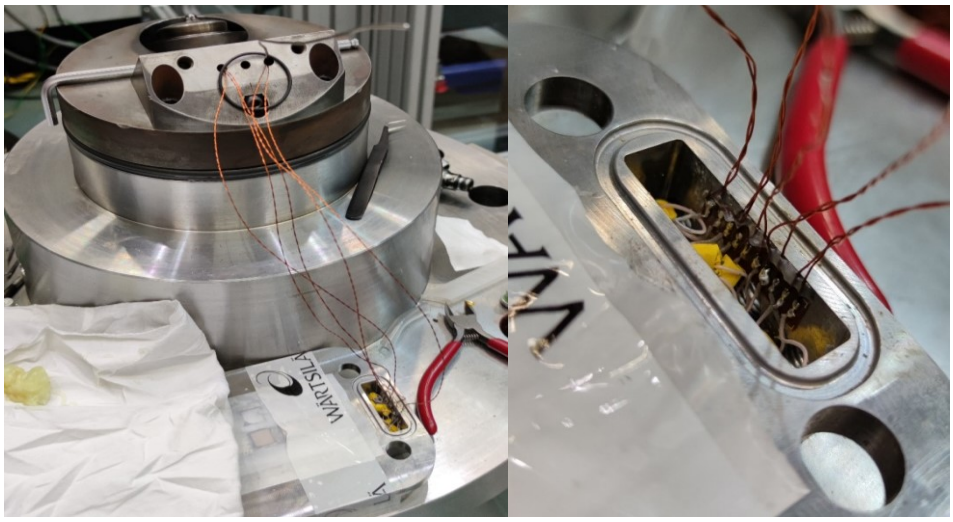

Figure 29. Soldered sensor wires to the soldering terminal and cable routes out of the OSCC.

## 3.4 Measurement setup and trigger management

Parallel measurements during the measurement campaign were synchronized to measurements stored in Dewesoft. It was decided that the trigger for the injector current signal would be optimal for synchronization due to controlling the injection spray. Devices receiving the control trigger can be divided into measurement signals and to control signals for laser, shutter driver, PMT, and injector that starts these devices at the correct time.

### 3.4.1 Measurement equipment

Measurement equipment and software used to measure heat flux during measurements were designed by Dewesoft (2021). Equipment used was Sirius XHS, which is designed for high-speed measurements. It can have up to 1 MHz sampling rate. Sirius XHS is a Data acquisition (DAQ) system. It is used for recording analog voltage and current signals that measure real word physical phenomena such as heat flux, pressure, and temperature. DAQ converts recorded data from analog signal to digital signal for post processing and

analysis. It is also possible to have digital input signals from other measurement devices. The model used can measure up to eight different analog and digital signals. Requirement for the measurement campaign was five analog channels for the GHFS, two channels for pressure and temperature inside the OSCC, and one for the injector control signal for trigger reference. Combustion sequence inside the OSCC was recorded for post analysis. These included gas filling inside the chamber, pre-combustion and spray combustion. Pre-combustion and spray combustion events took a total of 1.5 seconds. In total the previously mentioned sequences and the cooling of the chamber took on average 1.5 minutes to complete (Koivuluoma, 2022). Vacuuming the chamber for gas filling is the most time-consuming part of this cycle. Analyzing the vacuum sequence for heat flux was unnecessary and not included in the data. Recordings started from vacuum and ended after spray combustion.

Time of this spray combustion was estimated from engine data. The Wärtsilä 31 engine operates at a 750 rpm with an estimated diesel spray combustion event of 11 ms (Wärtsilä Corporation, 2023). Similar combustion event was replicated inside the combustion chamber. With 1 MHz sampling rate DAQ can have 1000 samples per 1 millisecond for each channel. Estimated file size with eight channels measuring at this sample rate would be 16 MB/s. Measurement event takes between 60 - 75 seconds meaning estimated file sizes would be around 0.96 – 1.2 GB. Channels for the current signal and thermocouple used lower sample rate to reduce file size. These signals did not require a high sample rate for post analysis. Thermocouple's sample rate was 10 kHz due to not having a fast response rate. Other applications that increase the final file size are any post processing done in the Dewesoft software. These include digital FIR filtering to reduce signal noise. Estimated file sizes from the measurement campaign on average were 0.9 GB and could go up to 4 GB from post processing changes. Only raw files from the measurement were stored.

For high frequency measurements it is recommended to have a sample rate that exceeds the recorded event to represent data in good resolution. Nyquist-Shannon theorem

states that at minimum the sample rate should be over twice the highest observed frequency. In addition, sample rate should be 100 times or more in high frequency measurements to be certain of the resolution when displaying the signal in time domain (Dewesoft, 2023). Converting the analog signal to digital has deviations that are caused by several types of distortions such as aliasing, quantization, and noise. Oversampling limits the effect of distortion to the signal.

Bitrate of the hardware also affects the resolution of the recording. DAQ systems overall use 8-bit resolution but for high–speed measurements require higher bitrate. As seen in Figure 30, the DAQ system converts the changes in the analog signal as either a negative or positive change. The resolution of the Analog-to-Digital converter (ADC) inside DAQ affects the similarity between the analog and digital signal. The chosen equipment, Sirius XHS, has a 16 – bit resolution. Digital signal with 16 – resolution has $2^{16}$ or 65 536 evenly distributed levels. Devices measuring between +/- 10 V can detect 300 µV change in analog signal. GHFS sensors used for this measurement will stay under -/+ 1 V range which allows the measurement channels to detect changes up to 30 µV.

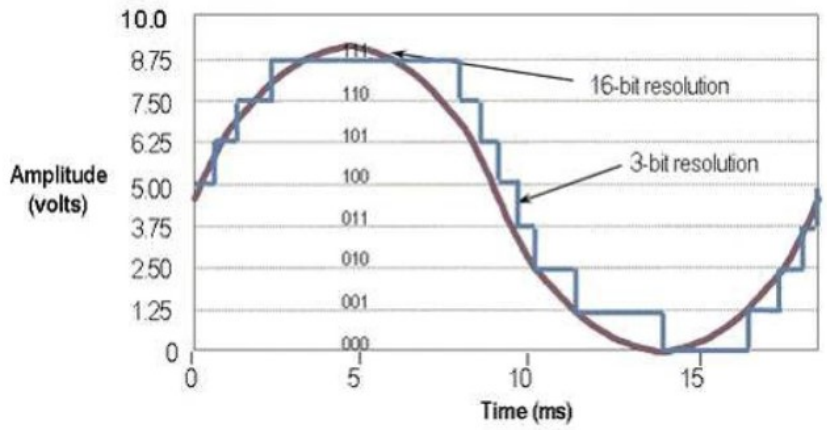


Figure 30. Resolution comparison of a digital signal.

### 3.4.2 Additional measurements

For this measurement campaign additional measurements would be done with addition to GHFS to assist with validating heat transfer caused by the spray combustion. These can be characterized in three different categories. First are video recordings for visual validation done with high-speed camera recordings with color and monochromic cameras in 50 kfps and 25 kfps respectively. These would be used to visualize the spray combustion from a single spray before hitting a surface and how the combustion would be affected by the plate. Furthermore, these recordings would show where the natural chemiluminescence caused by the combustion would be the strongest when impingement happens between the combustion and the plate.

Luminescence inside the chamber is the most interesting for the second category of measurements. In one of these luminescence is measured with a pyrometer where thermal radiance is measured in specific wavelengths. These measured signals can be then converted to temperatures by previous calibration done against a blackbody cavity (Sutton et al. 2021). Pyrometer was able to achieve a sample rate up to 250 kHz, but it was lowered to 100 kHz due to concerns of the recorded file size. It was concluded that the new sample rate would still be fast enough for a good resolution measurement (Sutton, et al. 2022). Combustion event with a W31 injector was expected to take 11 ms (Wärtsilä Corporation 2019). Another measurement done adjacent was with a laser pulse causing excitation of temperature induced emissions of photons that were captured with a photomultiplier tube (PMT). The measured signal required a high sample rate of 2 Gs/s for good resolution thus requiring a device capable of this such as an oscilloscope (Grahn 2021). The captured photon signal can be then converted to a temperature value. This measurement technique is called phosphor thermometry. Phosphor thermometry is measured by the phenomenon of phosphorescence where photons are emitted from a substance after being excited by an external energy source (Yen, et al., 2007). Grahn (2021) goes in more depth in the background work of how phosphor thermometry measuring works, preparation work, what was required to excite and capture the photon, and calibration done to convert excitation signal to temperature value. Spectrometer was

also added to measure wavelengths caused by the combustion. Results would help decide what best phosphor layer should be used to the measurement plate. Both phosphor thermometry and spectrometer are not continuous measurements from the combustion event thus cannot be synchronized the same way as the other measurements. Spectrometer gives a summarized range of luminosity wavelengths and its amplitude during the combustion process while phosphor thermometry measures temperature on the plate in fixed time. However, this temperature value can be used to compare, calibrate or to validate other measurements if successful.

Third category of measurements include GHFS and any other sensor that needs to be physically installed inside the OSCC to measure during the combustion process. These include thermocouple sensor and pressure sensor measuring ambient temperature and pressure inside combustion chamber and pressure sensor inside the pre-chamber. Pre-chamber in this case being where gas pipes from different sources would go before being added to the combustion chamber. Thermocouple and pressure sensors are also used as references for the pre-combustion event that was discussed in Chapter 3.1. Thermocouple sensors could not be used to measure temperature due to its response speed but rather was used as a reference for conditions before pre-combustion. Combustion chamber pressure sensor was also added for similar reasons but was also measured in high sample rate to see follow pressure during pre-combustion and combustion. Both pressure sensor and GHFS would have maximum possible measurement speed in Sirius XHS Dewesoft DAQ system which was 1 MHz per channel.

### 3.4.3 Trigger management

Trigger management was required due to several measurement and control devices. It is also required to synchronize measurement data from different sources. Main requirements for this trigger system includes that it is fast enough for sequences that happen during the combustion process which in this case is expected to be around 11 ms, it can manage to output several different signals, and have different offsets before or after the master signal is sent (Koivuluoma 2022). The master signal used was the control signal

for the injector. Offset used for the devices varied upon the usage. For example, the spectrometer used had a 2250 µs delay from the injector.

Due to being beneficial for future measurements done on OSCC, it was decided that the trigger management system would be implemented to the automation system used for pre-combustion and combustion sequences. Automation control system used was Speedgoat hardware and programming with MATLAB® and Simulink® (SpeedGoat, 2024). Up to one microsecond sample rate accuracy could be possible for the system. Designing of the trigger management system for OSCC and its setup and restrictions is discussed in more detail in Koivuluoma's (2022) work for the automation system. Cables used minimal length between devices and the Speedgoat to limit delays.

Almost all devices used during the measurement campaign were added to the trigger management system. Those not included were synchronized with devices that received a trigger signal. This was due to not requiring pre-trigger or was already storing data during pre-combustion. These included the oscilloscope that received a voltage signal from the PMT and the Dewesoft DAQ system. Figure 31 shows all devices under the trigger management system.

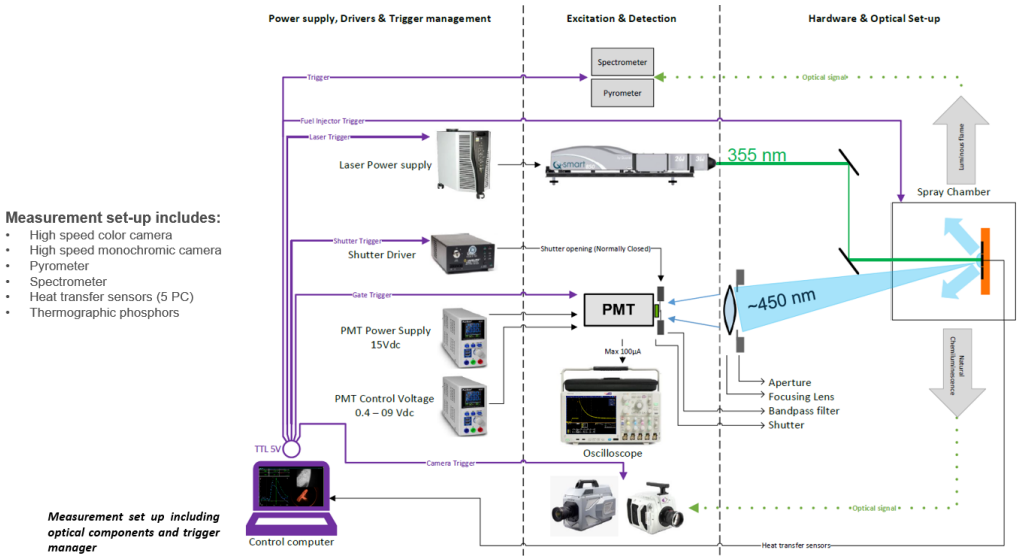


Figure 31. Trigger management system showing all devices receiving direct trigger signal from control computer.

Measurements done with Dewesoft were manually started due to interest in measuring chamber pressure during pre-combustion. Synchronization with other measurements was done with the measured current control signal. The signal would act as the reference 0 s point time for synchronization. Reference point would be triggered when rising edge current over 8 A was measured with a current clamp. Sample rate of the signal was kept at 500 kHz. Time delay was expected from the control module processing the fuel injector profile for the used injector. In addition, differences would also be seen with cable lengths between trigger manager and other devices. These were minimal and did not need to be factored into synchronization inaccuracy. Performed synchronization enabled post-processing with Dewesoft to include data from high-speed cameras and the pyrometer.

### 3.4.4 Hot combustion validation and instrumented corner module testing

Before any testing was done with the instrumented plate there was planned validation testing for hot combustion inside OSCC. During this the injector used for the measurement campaign would be in use, which would allow testing of the measurement setup done with Dewesoft. This was also the first possibility to add an instrumented corner module with GHFS to measure and see how it would survive the hazardous environment inside the chamber during the combustion sequence. Concern was that the event was too hazardous for the sensor that it would break from consecutive combustions.

As stated in Chapter 3.1 pre-combustion especially showed high pressure rise rates that could break the sensor or instrumentation done on the corner module. Either the adhesive gluing the sensor to the corner module would break or that it would melt from heat and break the soldering joint between the sensor wires and sensor. Testing done during hot combustion validation would not give any data from spray combustion. Hot commissioning also had a high-speed camera in use with the injector current signal as the master trigger signal. Thus, would allow changes to be made for the triggering system, if necessary, before starting the measurement campaign with the alignment plate.

### 3.4.5 Alignment and initial testing with a plate

Before installing the instrumented plate with heat flux sensors, it was important to align the plate correctly for spray combustion. The impingement point of the spray required to be in the center point of the plate where GHFS #3 would be installed. A dummy plate was installed with the same specifications without the sensor pits to see where spray combustion would hit the plate. This would allow corrections to be made, if necessary, by moving the placement of the instrumented plate. To prepare the dummy plate a layer of white paint was painted to emphasize combustion area applied to the plate. There were concerns that the plate would not show any differences on the surface of the plate even with fuel burning directly to it. Installed alignment plate can be seen in Figure 32. The instrumented corner module with GHFS would also be installed to the chamber for further testing. Measurement setup can be seen in Figure 33 where both high-speed cameras, pyrometer and spectrometer are installed.

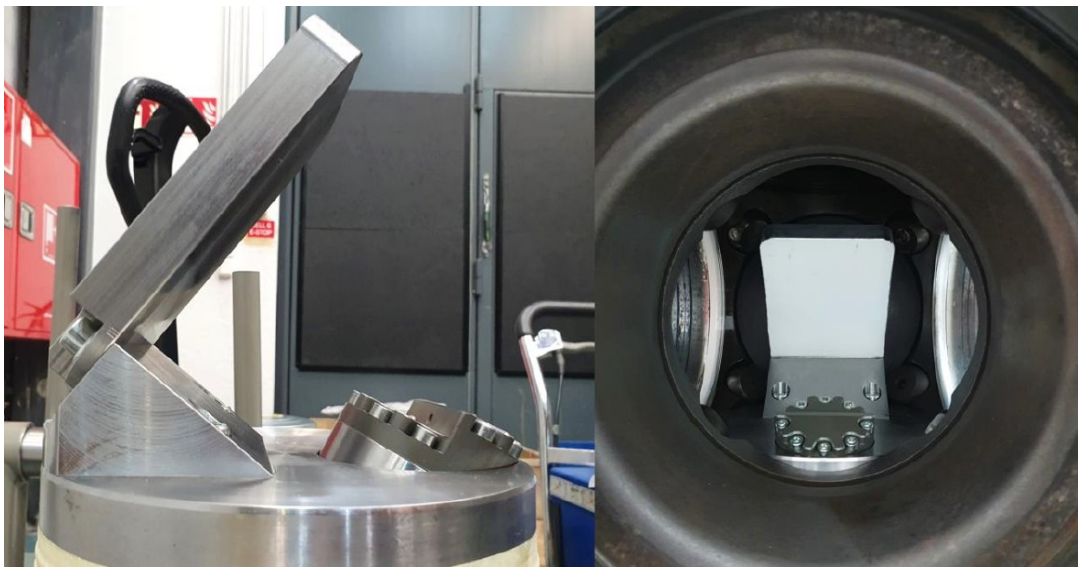

Figure 32. Alignment plate installed inside the OSCC.

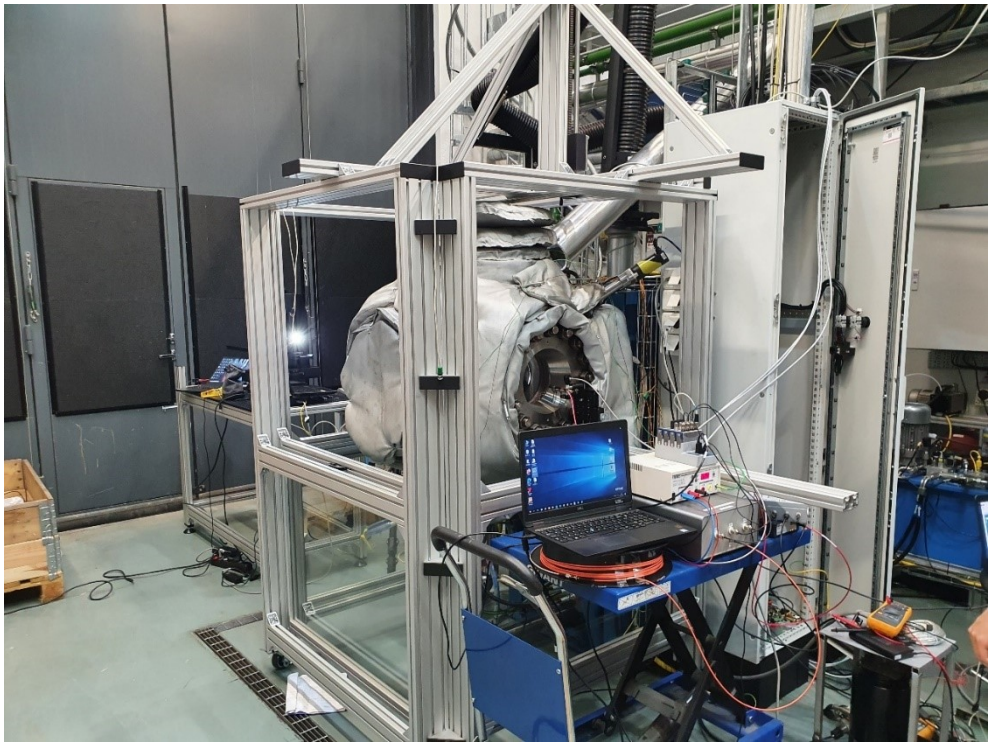

Figure 33. Measurement setup during alignment tests. Pyrometer and spectrometer on closer window and high-speed cameras on the other side.

The alignment test was also the first measurement campaign that was done after the OSCC was validated for hot combustion testing, which meant that there was interest to see how OSCC functioned with continuous testing. Using the videos captured by the cameras it would be possible to see targets and times of interest during spray combustion. These were for the pyrometer and phosphor thermometry measurement. The high-speed cameras would allow us to see where we would see highest exposure of flames before impingement to the plate. For phosphor thermometry measurement more concern was for limiting noise from wavelengths caused by the natural chemiluminescence from the diesel spray (Grahn, 2021). If possible, measurement would be taken when luminosity from the flame would be minimal between the PMT sensor and plate. Grahn (2021) describes similarities with diesel spray and the emitted phosphorescence signal wavelength that could weaken received signal from the PMT.

For these measurements both high speed cameras and pyrometer were triggered simultaneously with injector current signal and spectrometer with 2250 µs delay. Delay was to diminish impact of pre-combustion to the measurement. In addition, injection spray was expected to be seen with a delay from the injector current signal. Pyrometer measurement target was placed directly next to the impact point of the center of the spray where it would hit the surface plate.

### 3.4.6 Instrumented plate measurement setup

Installation of the instrumented plate was prepared as described in Chapter 3.3.5. The instrumented plate was painted in specific spots with mixtures of phosphor. One of these areas painted was GHFS#5. Modifications were also made to protect the sensors from pre-combustion done inside the chamber. Reasons for the changes were due to the instrumented corner module measurements discussed in Chapter 4.1. Main issue was that the pre-combustion inside the OSCC could be too hazardous for the adhesive. It was decided to cover one of the sensors with a 0.3 mm steel plate that was spot-welded. To electrically isolate the sensor from the steel plate, a 0.05 mm thick mica sheet was placed between them. Spot-welded plate and painted areas for phosphor thermometry can be seen in Figure 34.

Measurement setup was similar to alignment test, but pyrometer position was changed due to interest to measure further away from the plate. Goal was to correctly measure the end point of the spray from the injector. It was not possible next to the plate due to flame shape staying there longer during combustion spray sequence. In addition, a laser was used to energize phosphor painted on the plate. New setup can be found in Figure 35.

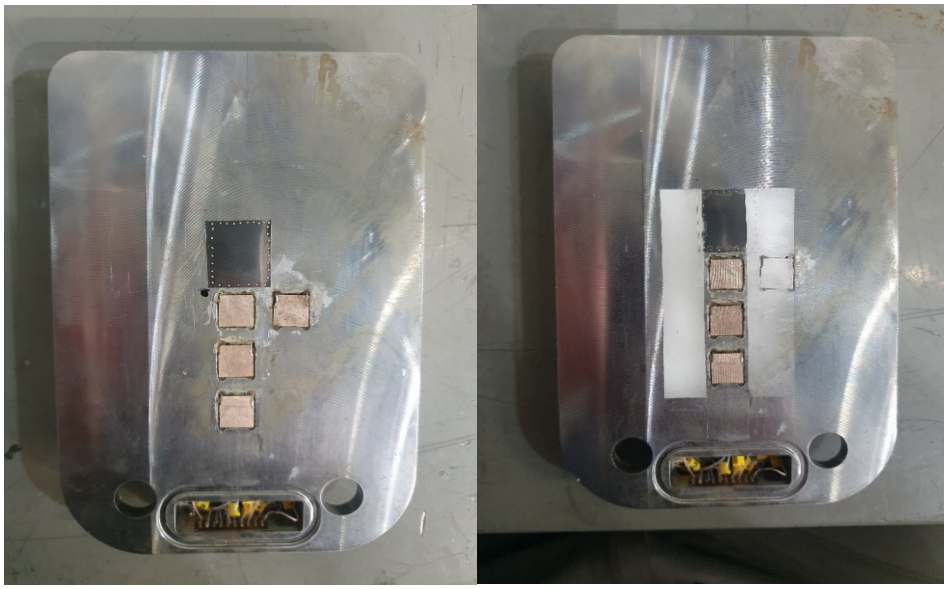

Figure 34. Phosphor paint and steel plate added to the instrumented plate.

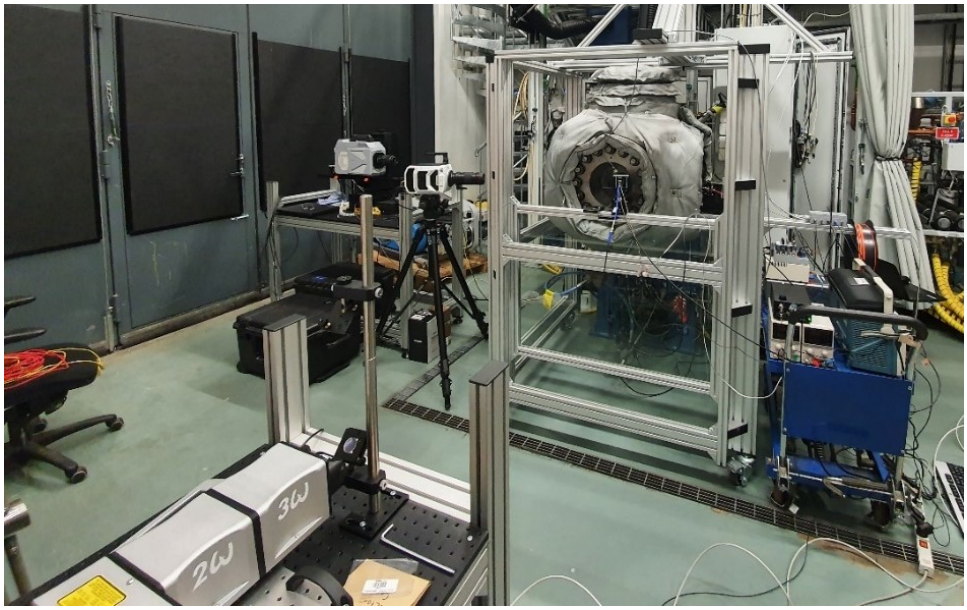


Figure 35. Measurement setup used with an instrumented plate. Laser on the corner added to the previous alignment test.

# 4 Results

## 4.1 Instrumented corner module test

Hot combustion test was performed to validate OSCC for spray combustion testing. During these tests instrumented corner module was installed to the chamber. Before starting with injected sprays for combustion pre-combustion tests were done. Figure 36 shows the first pre-combustion where the instrumented corner module with GHFS was installed. Peak pressure measured was 53 bar during the combustion sequence while GHFS sensor was measuring –66 kW/m$^2$. Due to the noise, it was not possible to use given sensitivity for the sensor to approximate heat flux correctly from the precombustion. The measured signal from the GHFS had sizable noise that was caused by ground loop. Filtered recording can be seen in Figure 37. Pressure rise rate was calculated to be 1350 bar/s.

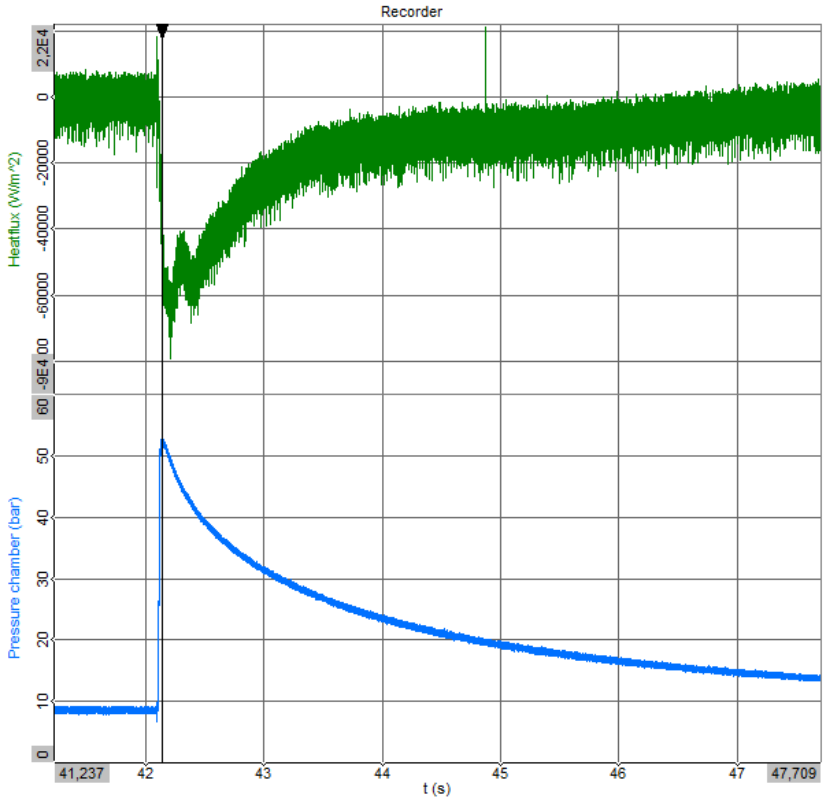


Figure 36 Measured Heat flux during hot combustion validation. Pre-combustion peak pressure was 53 bar.

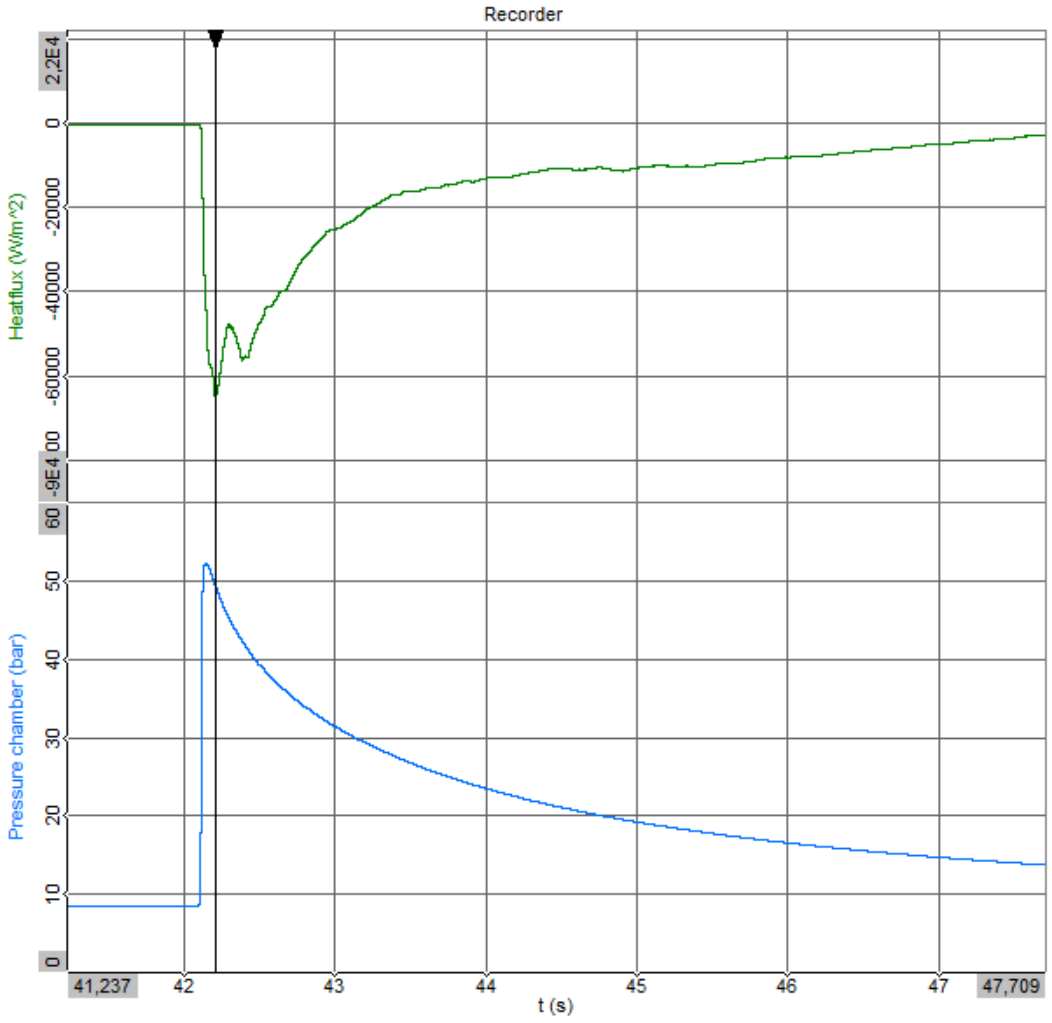


Figure 37 Filtered signal from hot combustion validation.

The instrumented corner module was inspected after the pre-combustion sequence was measured. There were concerns that the sensor was broken due to negative heat flux from pre-combustion inside the chamber. Removal of the instrumented corner module showed that instrumentation had failed. Figure 38 shows the sensor had ripped off itself from the sensor pit. Most of the adhesive binding the sensor was also gone from the sensor pit after the pre-combustion. Only a small amount of the adhesive layer could be still seen on the surface. The sensor was unable to be found for further inspection inside the chamber. Most likely it was removed from the chamber during exhaust valve opening that removed existing gases from the OSCC.

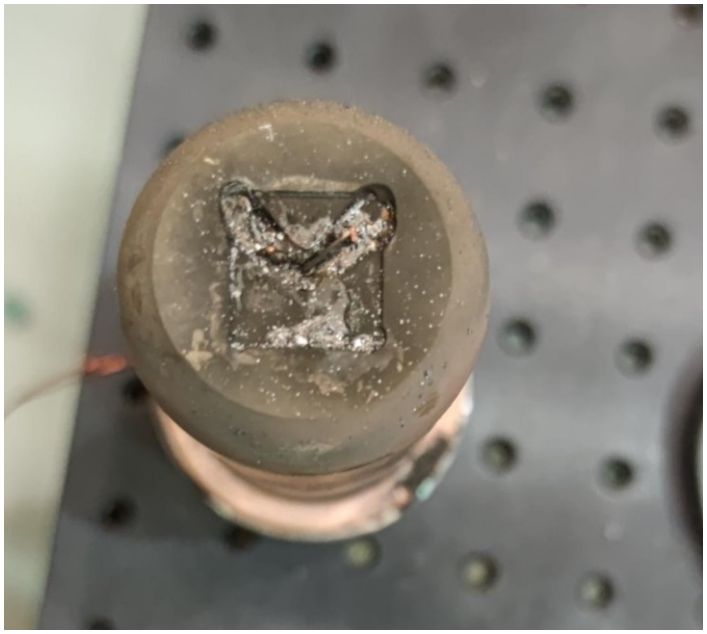

Figure 38 Instrumented corner module after pre-combustion.

Testing was continued after installing a new instrumented corner module with the same instrumentation procedure discussed in Chapter 3.3. The prepared instrumented corner module is shown in Figure 39.

Figure 39. Modifications done to the corner module. Teflon tape was added to the walls and bottom of the sensor pit before applying the adhesive. Unnecessary tape was removed before installation to the OSCC.

Similar issue was seen with the new instrumented corner module during these tests that showed unreliable signal from the GHFS sensor. In this case both positive and negative heat flux were measured. Using Teflon material to isolate the sensor from the corner module did not work as intended. Figure 40 shows filtered signal from the first combustion sequence after installing the corner module. Similarly to the previous test the GHFS seemed to break after first pre-combustion. Detonation wave caused by the spark plug was measured to be 1450 bar/s during pre-combustion. The sensor was not found from the chamber like with the previous measurement.

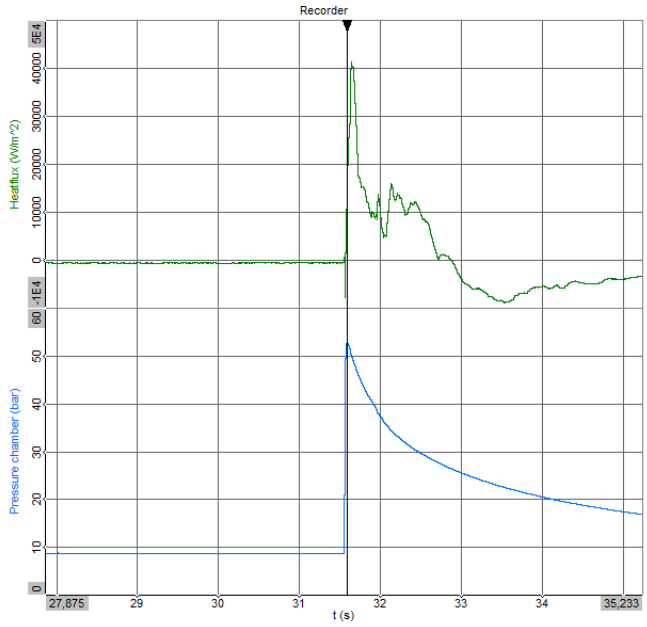


Figure 40. Filtered hot combustion validation with 53 bar measure from pre-combustion. The sensor can be seen breaking from pre-combustion.

The alignment test used a third instrumented corner module. Sensor pit of the corner module was widened due to issues raised while testing the durability and functionality of the GHFS. After installation similar issues were seen as before. Damage done to the instrumented corner module after the alignment testing was inspected and can be seen in Figure 41. Some adhesive is still visible on the surface of the sensor pit but most of it has burned away or broken to pieces from pre-combustion.

Figure 41. Corner module following alignment test.

Trigger reference from injector current signal was used successfully to synchronize high-speed camera recording. An example of synchronized recording can be seen in Figure 42 where spray combustion hits the surface of the plate. Both color and monochromatic videos, pyrometer, injector current signal and chamber pressure were recorded. For the alignment test the chosen combustion pressure for spray combustion was 88 bar. Start of Energization (SoE) of the injector was used to have a comparable starting point to compare different measurements. Time after SoE (aSoE) was used to indicate at which point in time something was recorded during the combustion sequence. For example, Figure 42 shows combustion spray shape at 7 ms aSoE.

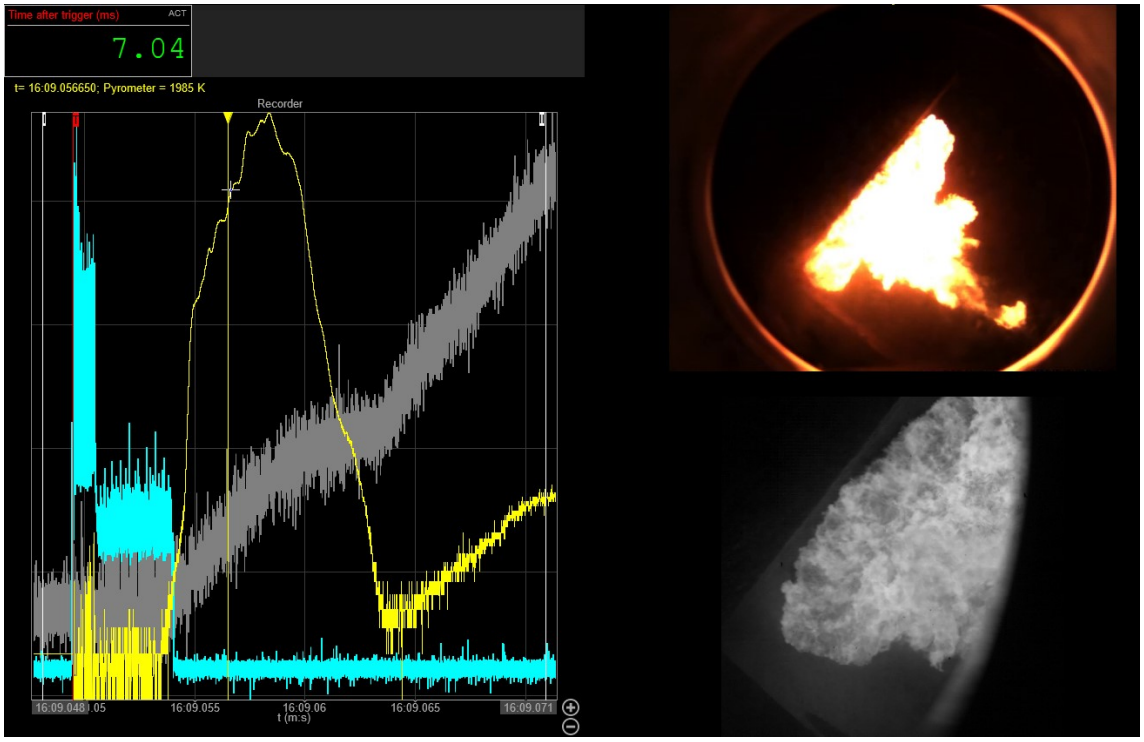


Figure 42. One of combustion sprays recorded during alignment test. All measurements done were incorporated together using injector Start of Energization (SoE) as the start reference. Recorded signals shown are injector control signal (cyan), pyrometer (yellow) and chamber pressure (gray).

Variety of combustion spray shapes were seen during the alignment test which also affected temperature recorded with the pyrometer. Thermal radiation was recorded in three different wavelengths 850 nm, 1050 nm and 1300 nm that showed different results. The most accurate was 850 nm and is displayed on all recordings. More in depth analysis and preparation work can be read on a report that was written with assistance of the National Physical Laboratories (NPL) in the UK. Report was part of a larger project of Dynamic Pressure and Temperature (DynPT) where new measurement techniques are discussed in detail (Sutton, ym., 2022). From the seven successful recordings an average shape could be calculated which is displayed in Figure 43. Peak temperature was estimated to be 2100 K at 9 ms aSoE. Picture taken at 7 ms after SoE (aSoE) from color high-speed camera recording displays placement of the pyrometer measurement point.

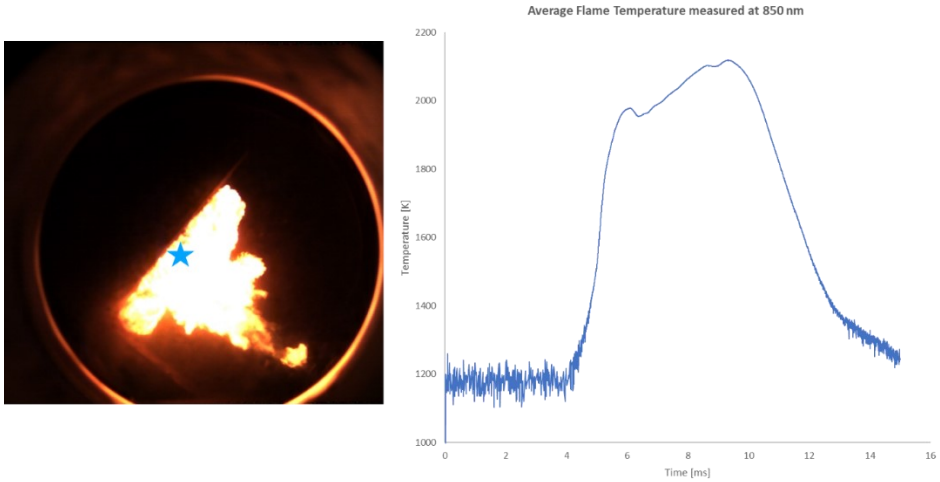


Figure 43. Recording of the pyrometer during the alignment test. Picture taken from a color high-speed camera at 7 ms aSoE.

After consecutive spray combustion were injected into the plate it was inspected to check if there was any deviation between center of the spray and GHFS#3 position on the plate. Approximate center point was measured and shown in Figure 44 that places it close to GHFS#3. Spray combustion center point has an offset to the right corner from the sensor pit. It was deemed accurate enough to continue with the same alignment setup when installing the instrumented plate. Variance was expected between sprays where it would hit the plate. Thus, improvement to accuracy from moving the position of the plate on the center point position would require additional consecutive combustion sprays in different alignment setups.

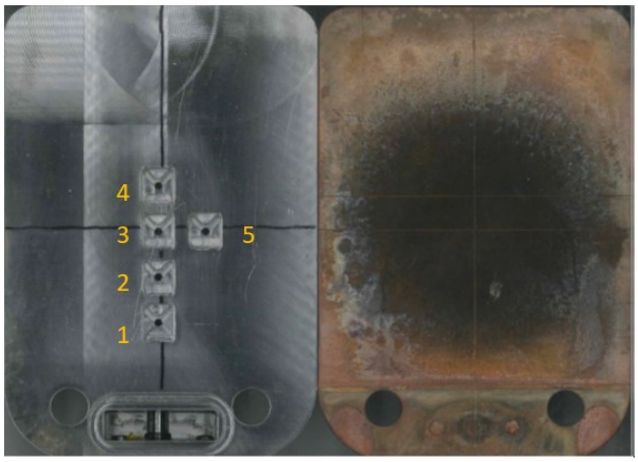


Figure 44. Center position of the diesel spray. Result after being exposed to 20 diesel com-bustions inside the OSCC.

## 4.2 Instrumented plate test

The combustion setup for the instrumented plate was the same for combustion sequence as with the alignment test. In other words, an injection similar to 59 % load in W31 was performed in 88 bars with LFO for comparison data. Goal of the measurement was to get good measurement data from the attached GHFS to the plate and other measurements done parallel during the test. Concern was that the sensor instrumentation would not be able to survive several combustion sequences inside the chamber. The pre-combustion sequence caused rapid pressure shockwaves that would break the adhesive layer holding the sensor in the sensor pit. GHFS#4 was shielded with a spot-welded plate to protect it from the pre-combustion sequence. Due to the time schedule, it was not possible to do another instrumented plate to try other adhesive materials. The goal was to have as many successful combustions as possible from the start before adhesive used would break.

During the alignment test the pyrometer was measuring directly next to the surface of the plate. It was decided to move the measurement point to measure further from the mushroom cloud shaped flame seen in Figure 43. Placement for the new measurement position was decided to be around 4 cm away from the surface of the plate. New position can be seen in Figure 45.

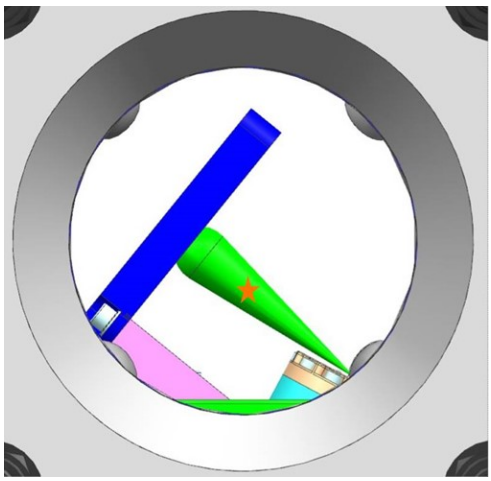

Figure 45. New position for the pyrometer during instrumented plate measurements.

In total 30 combustion sequences were done before all GHFS were broken. From these 15 had successful spray combustions that could be used to measure heat flux. Success ratio during the tests was due to issues with self-ignition during the gas mixing before pre-combustion. An example of a successful combustion measurement is shown in Figure 46. Similar issues with noise were measured in all sensors due to ground loop effect. Peak-peak noise before combustion sequence was measured to be between 5-10 mV for all sensors except sensor 4 with over 33 mV peak-peak noise. Sensor 4, which had a spot-welded steel plate cover that can be seen in Figure 46 also did not react during the combustion sequence from heat transfer.

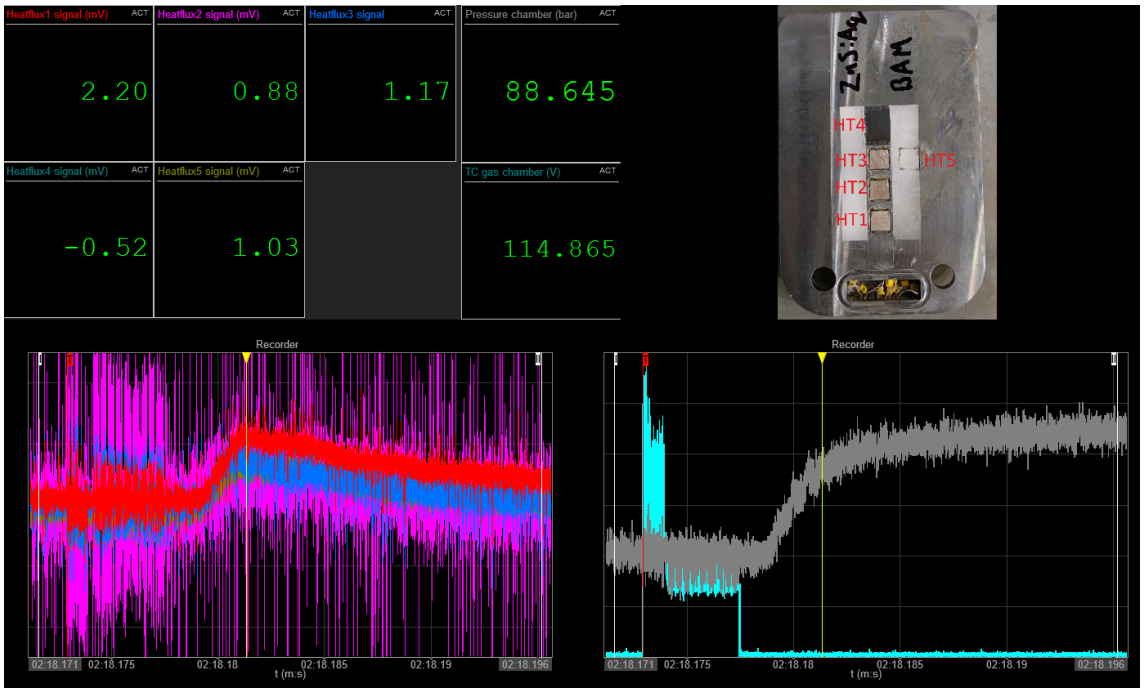


Figure 46. Combustion spray recorded during instrumentation tests. Upper left corner shows digital values of all GHFS signals and chamber temperature and pressure. Upper right corner shows the sensor locations. Bottom left corner shows noisy GHFS signals and the right corner shows injector control signal, cyan, and chamber pressure, gray.

Low pass filter with a cutoff frequency of 1200 Hz was applied to remove noise from the signal in all measurements recorded. Setup used for filtering can be seen in Figure 47. An example of filtered data can be seen in Figure 48 from combustion spray. Data shows no reaction to the heat transfer measured from the GHFS #4. Minimal offset can also be

seen from other sensors between 0 – 0.3 mV while peak voltage was different depending on the sensor position and combustion sequence.

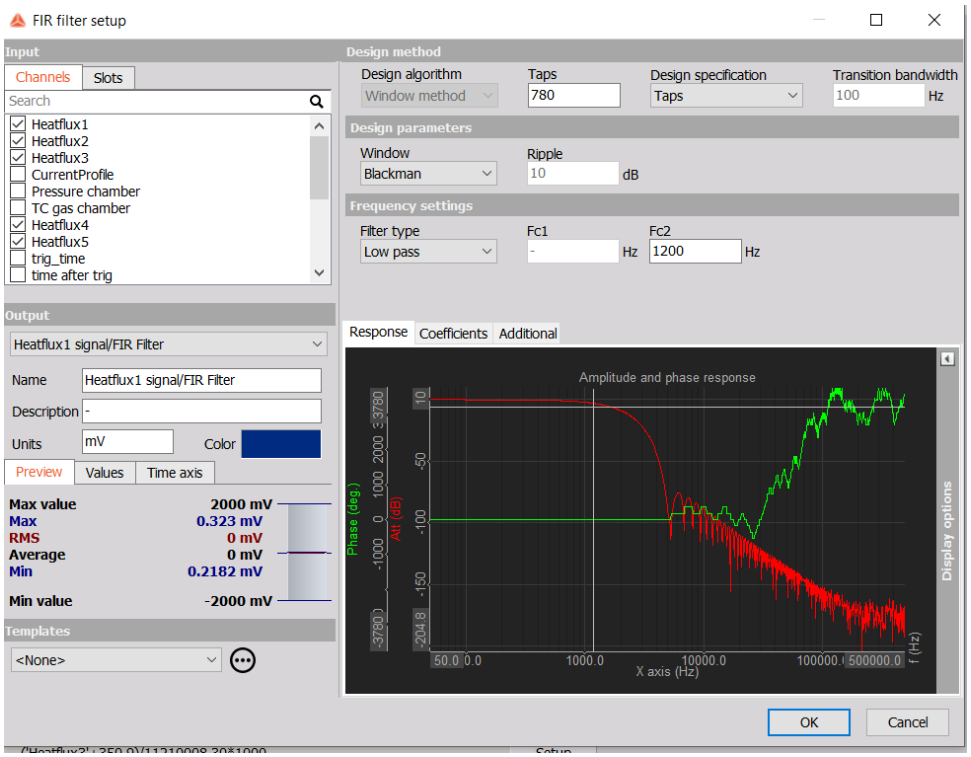


Figure 47. Filter setup for the GHFS. Low pass FIR filter with cutoff value 1200 was applied.

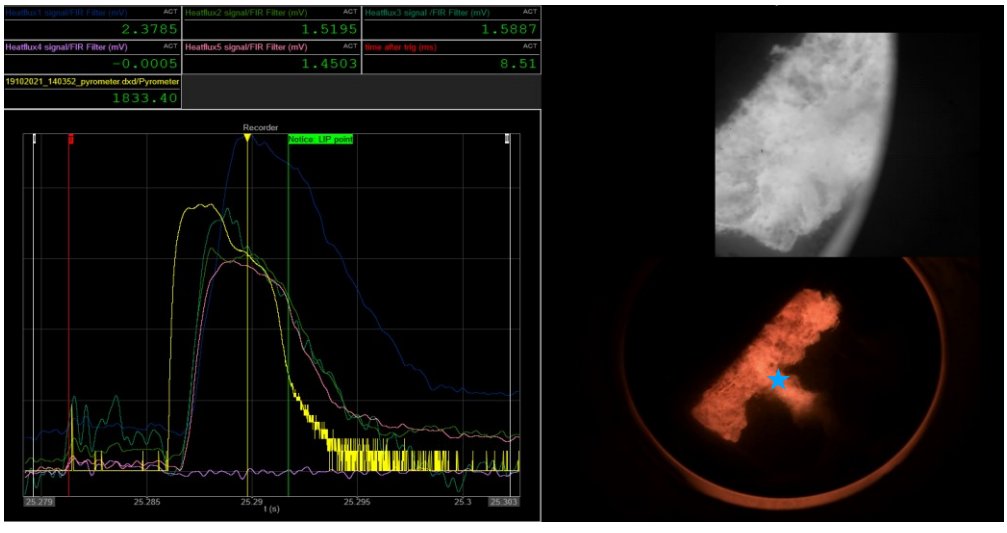


Figure 48. Filtered signal from all GHFS. Added a pyrometer signal together with GHFS sensors. High-speed cameras.

Highest voltage was measured consistently in GHFS #1 in all combustions recorded. From color high-speed camera recordings such as Figure 49 it is possible to see that in the region where GHFS #1 was placed the amount of burning diesel spray is also the highest. GHFS #2 and #5 showed similar peaks while GHFS #3 that was directly in the center of the spray had 0.2 – 0.3 mV higher peak voltage. Depending upon spray combustion, the peak signal for GHFS #1 was measured between 8.6 – 9 ms, for GHFS #2 and GHFS #5 at 7.5 – 7.9 ms, and for GHFS #3 between 7.2 – 7.6 ms. From pyrometer data peak flame temperature was reached between 5.5 – 7 ms.

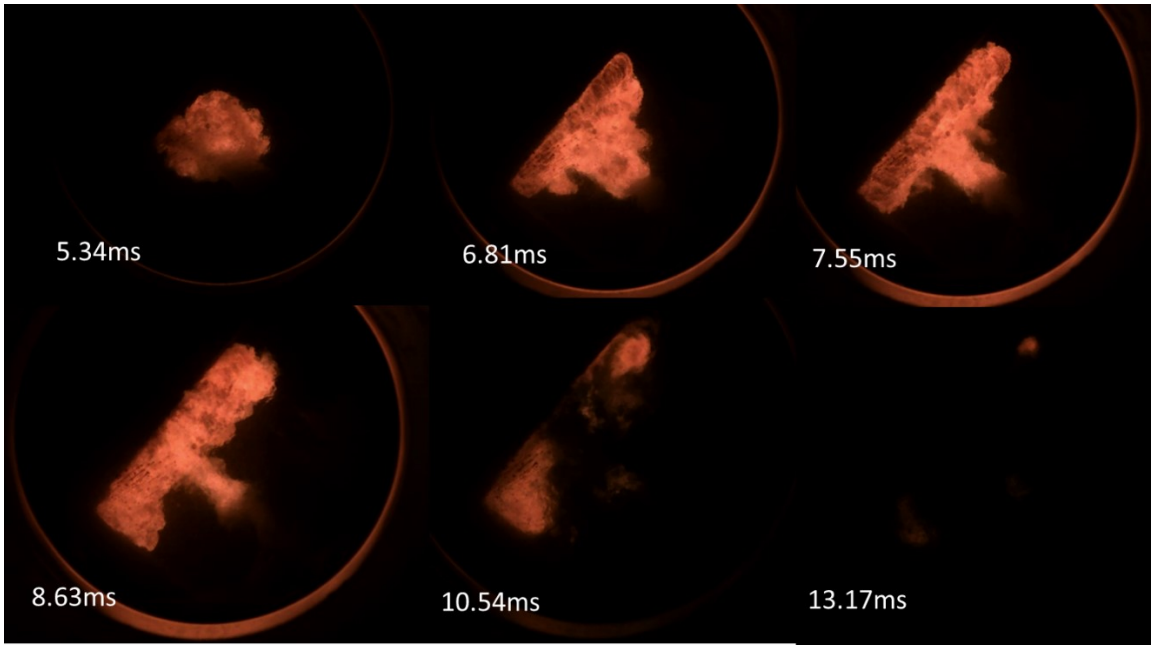


Figure 49. Combustion spray during combustion sequence after SoE.

From the 15 successful combustion sprays 11 could be used to calculate the average voltage signal for each sensor position. From these the signal shape for all the sensors can be seen in Figure 50. In addition, a similar average calculation was calculated from pyrometer data and added from these measurements. Calibrations done to the sensors were obsolete due to the high signal noise caused by the ground loop. Calculations were done from the filtered signal to reduce impact from noise to allow recalibration calculations to be done if possible.

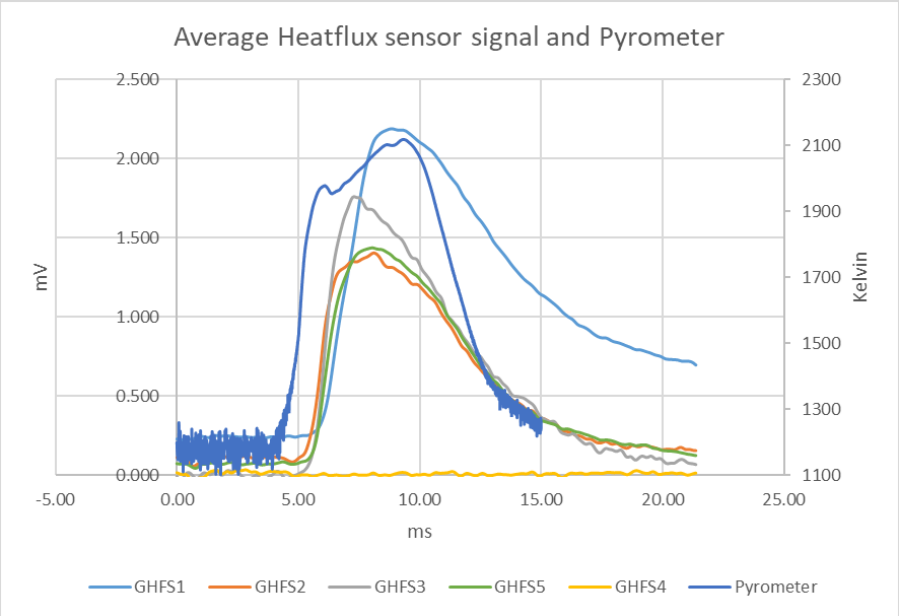


Figure 50. Average heat flux sensor signal and pyrometer temperature from eleven combustion sprays.

During 29th combustion sequence first damage was recorded for GHFS #5 that showed a similar data trend that was seen during corner module testing when a sensor broke. Figure 51 shows the instrumented plate and the sensors after the 29th combustion sequence. GHFS #5 was not glued to the plate anymore and GHFS#3 was loose. The chamber was inspected for GHFS #5 but was unable to be recovered for further inspection. Sensor was most likely lost during the exhaust procedure. When inspecting the other sensors, it could be seen that the adhesive layer for the GHFS #3 had broken and no longer was holding the sensor in place. The sensor was kept in place by a solder joint connection between the sensor wires and the sensor. It was decided that the sensor would be removed for further examination to estimate exposed temperatures that the sensor subjected to. GHFS #2 and GHFS #1 also had visible damage to the adhesive layer next to the walls. Both sensors were able to handle one more combustion sequence before breaking. Both sensors were able to be recovered from the chamber after inspection. The GHFS #4 was left inside the cover and testing was continued to finish the instrumented plate campaign.

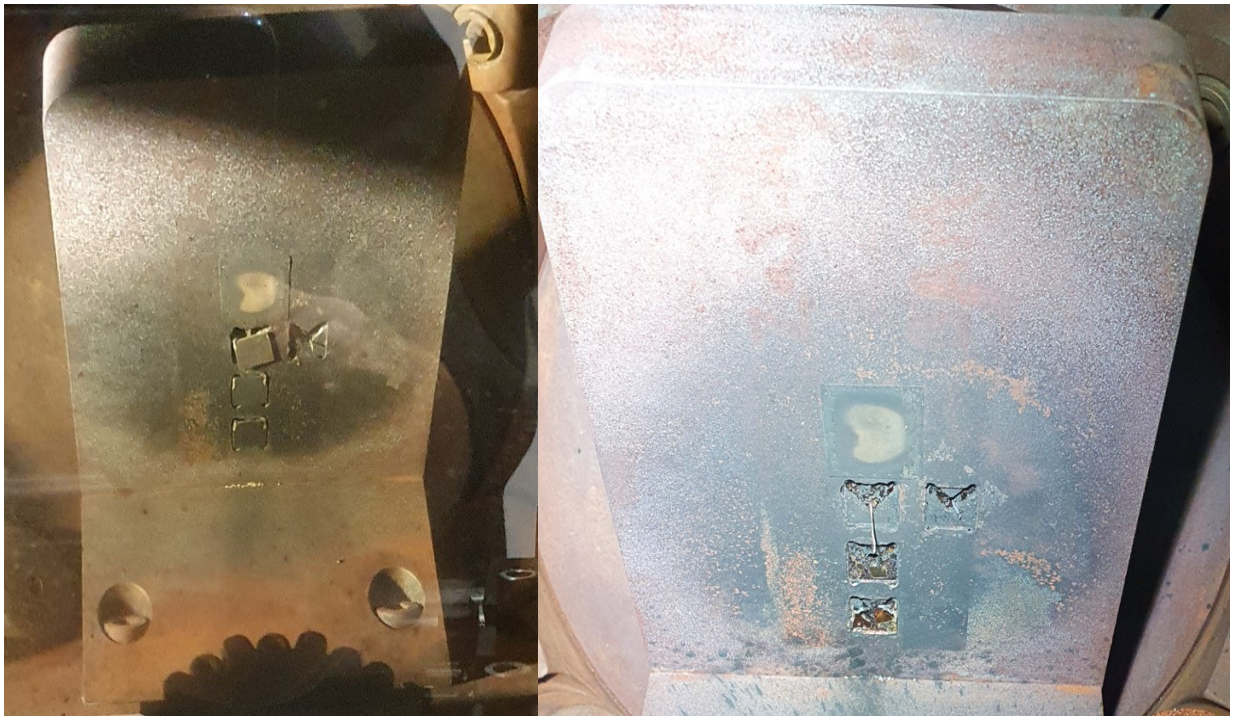

Figure 51. Instrumented plate after 29th and 30th combustion spray. GHFS #3 was removed after 29th combustion and GHFS #1 and GHFS #2 after 30th combustion.

During this the plate was exposed to 16 combustion sprays with n-heptane fuel that was used to measure the phosphor coated instrumented plate in less noisy environments measurement signal measured by the PMT. Position of the measurement point was also changed from the GHFS #5 position to the center point of the combustion spray, which in this case was GHFS #3. Timing of the measurement capture was also changed from 10.54 ms aSoE to 10.93 ms aSoE to have less background noise from combustion flame.

After the instrumented plate was removed it was noticed that epoxy sealing used to cover the cable route inside the plate was damaged. As seen in Figure 52 epoxy sealing had moved from inside the cable route and was pushed by the pressure difference between the chamber and environment. Otherwise, no visible damage was seen in the soldering terminal or cable route. Examination results done to the collected GHFS showed that the surface temperature on the instrumented plate had reached at least +500 °C due to oxidation visible on the sensor (Mityakov, 2021). When inspecting the soldering joints between the sensor and the sensor wires no visual damage was seen. Sooty surfaces can be seen on both sides of the sensors. Example is shown in Figure 52.

Soldering joint side of the sensor underside was exposed more to flame. Adhesive material and Teflon can be still seen attached to the sensor.

Figure 52. The soldering terminal of the instrumented plate with epoxy sealing pushed to the wall. GHFS #3 visual inspection with oxidation seen in the metal.

When removing GHFS #4 from the plate, the adhesive layer had to be damaged. Less amount of damage was seen compared to the others on the adhesive layer side of the sensor. As seen in Figure 53 no soot was seen under when compared to the other sensors.

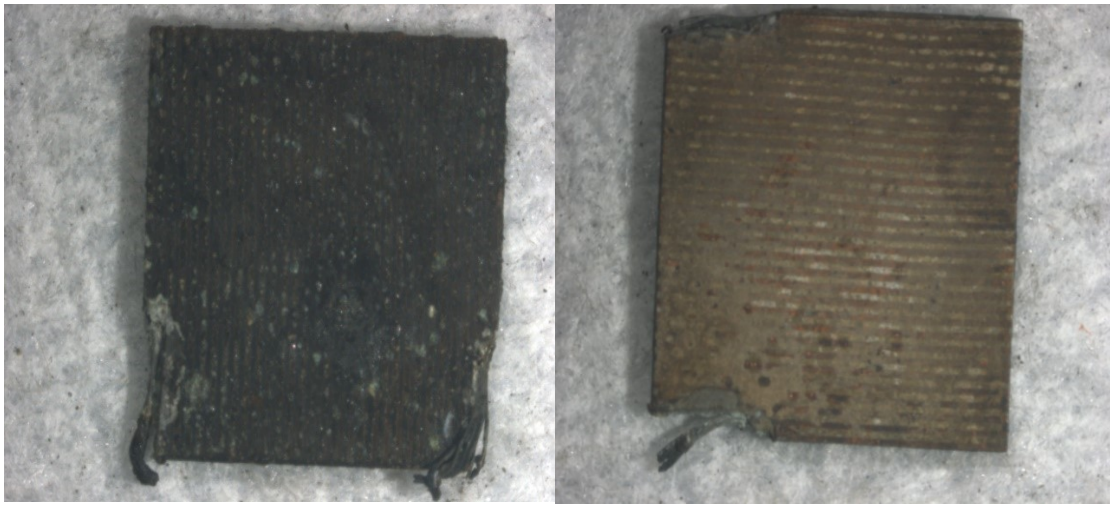

Figure 53. GHFS #4 after removal under the spot-welded cover.

After examination, the GHFS's were sent for recalibration to calculate new sensitivity after rewiring. Recalibration used seen oxidation and the gathered average voltage data from the spray combustion. From these an approximation for the sensitivity calculated from the following equation

$$S = 4.7806 * e^{-0.011*T_w}, \quad (8)$$

where S is sensitivity and $T_W$ is wall temperature. The heat transfer and heat flux could be calculated from the following equation

$$Q = E/(S * A), \quad (9)$$

where Q is heat transfer, E is measured voltage, S is sensitivity and A is sensor area. Calculations assumed that sensitivity was constant during the spray combustion Figure 54 shows heat flux approximation when the peak wall temperature is assumed to be 880 K.

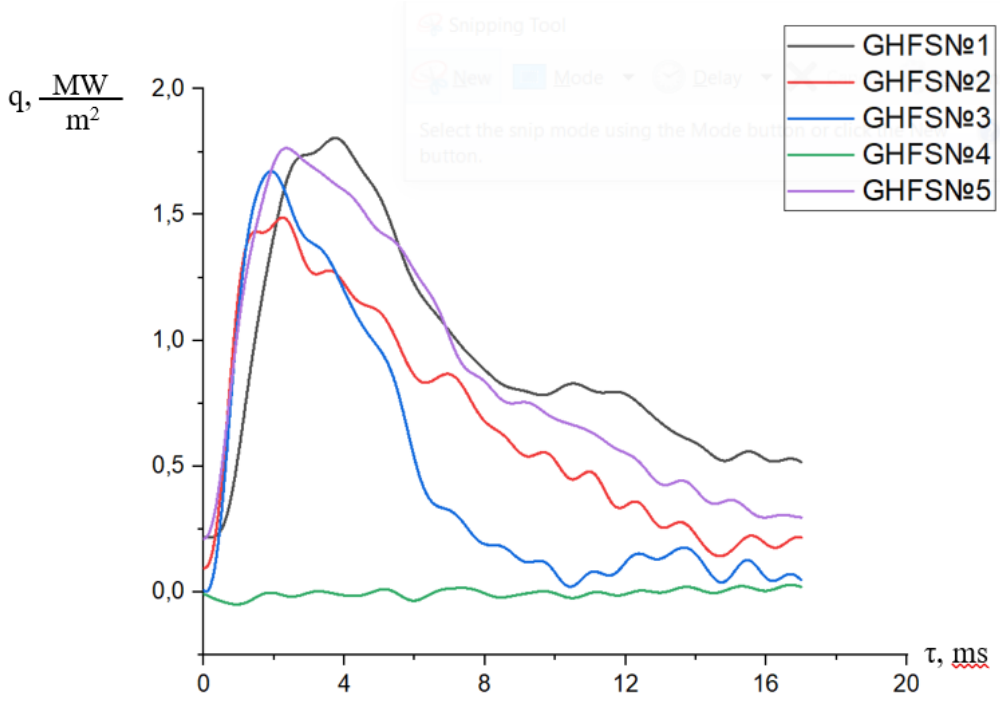


Figure 54. Heat flux (MW/m2) approximation on the Y-axis with constant sensitivity. X-axis shows time (ms) after SoE. Peak temperature for the wall was assumed to be 880 K (Mityakov, Sensitivity recalibration for sensors, 2021).

Reference surface temperature that could be compared to oxidation reference was received from Light Induced Phosphor (LIP) measurement results with n-heptane as fuel.

Measurement point for this measurement was at 10.93 aSoE. Decay time measured during the measurement campaign is displayed in Figure 55 From calibration measurements done to decay times captured by the PMT estimated average temperature was 880 K with lower limit of 850 K and upper limit of 935 K (Grahn, 2021).

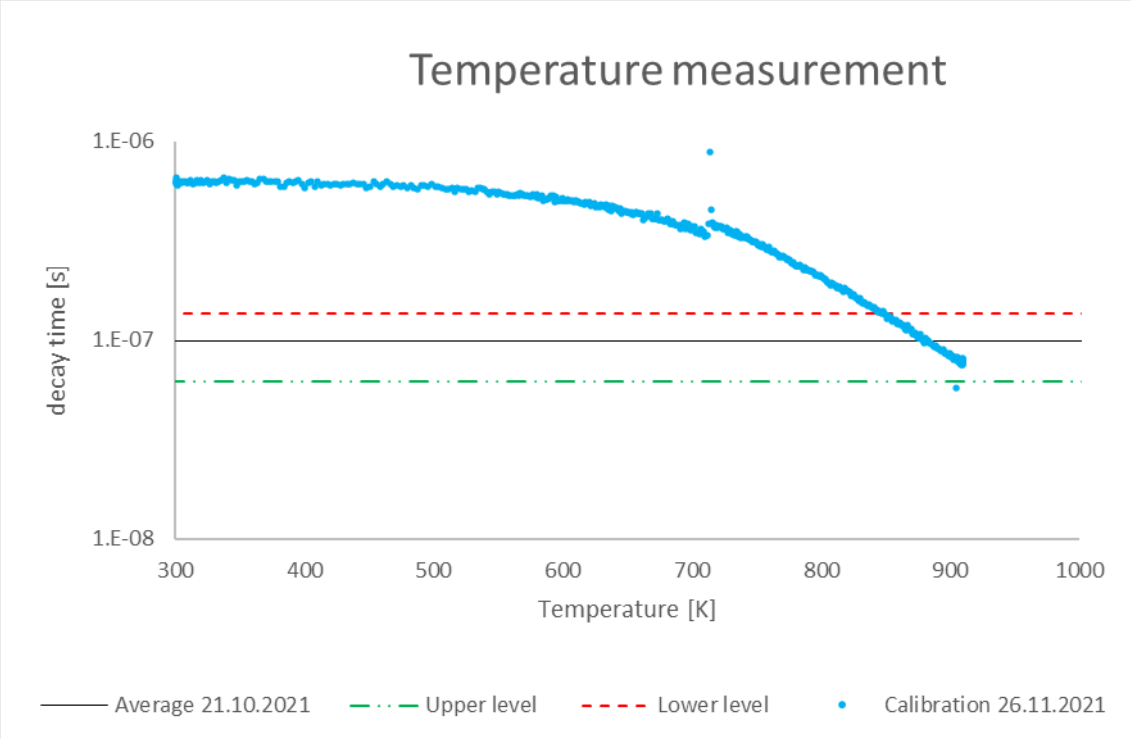


Figure 55. Temperature correlation between measured decay times and calibration points (Grahn, 2021).

From the measured 880 K temperature at 10.93 aSoE new heat flux approximations could be calculated. If assumed that the peak surface temperature was similar, then calculated sensitivity would be 6.0 µV/W. Alternatively, the peak surface temperature could be estimated from the measured heat flux signal. If the surface temperature would follow similar trend as the measured GHFS #3 signal, then peak temperature would be 950 K. Below both scenarios are displayed. Figure 56 shows the first scenario where peak temperature was assumed to be 880 K for all sensors. Second scenario is displayed in Figure 57. For calculations sensitivity was kept constant and peak temperatures was 950 K for all sensor positions.

Highest heat flux was measured with GHFS #1 and GHFS #3 has the second highest peaks while GHFS #2 and #5 have similar values. Similar estimation was discussed when planning the placement of the sensors where highest heat flux would be measured at GHFS #3 while similar values would be measured with similar length away from the center of the spray. GHFS #2 and GHFS #5 are the same length away from the spray center. The highest peak was assumed to be reached with GHFS #1 not with GHFS#3. No data was able to be measured from the GHFS #4 with the spot-welded cover that was placed due to concerns from pre-combustion detonation waves breaking all sensors. It was the only sensor that was able to survive without significant damage to the sensor itself. Having a cover to protect the sensor could be a possibility but some issues remain with measured voltage. Due to lowered voltage from heat flux with additional cover it is paramount that the sensor is electrically isolated to have as strong as possible signal strength. Furthermore, it is required that there are no air bubbles between the cover and the sensor or eventually the cover would break from pressure.

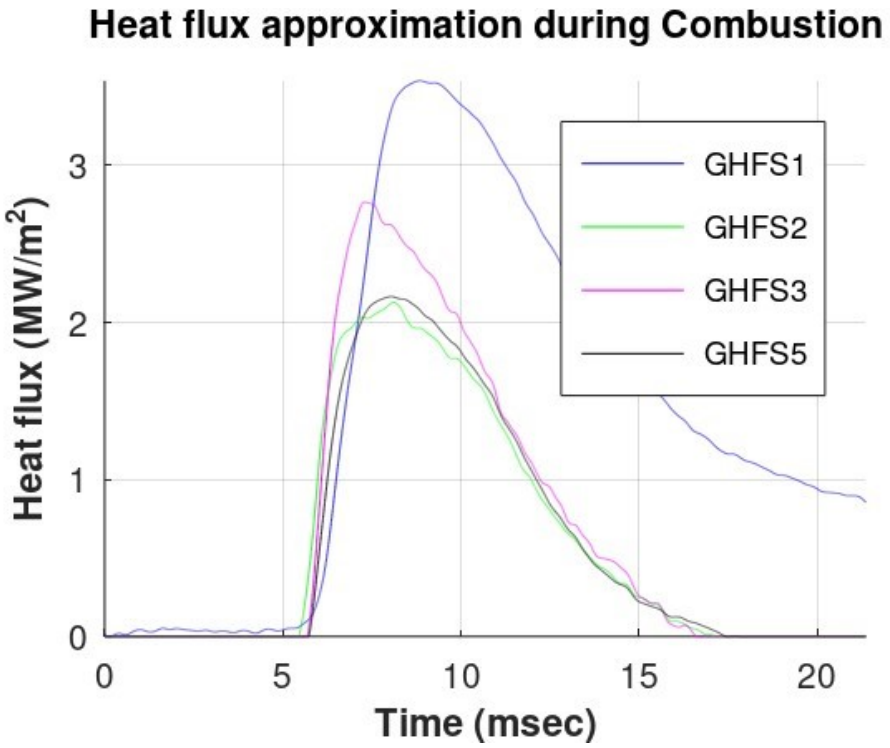


Figure 56. Heat flux approximation with constant sensitivity. Peak surface temperature was assumed to be 880K for all sensor positions.

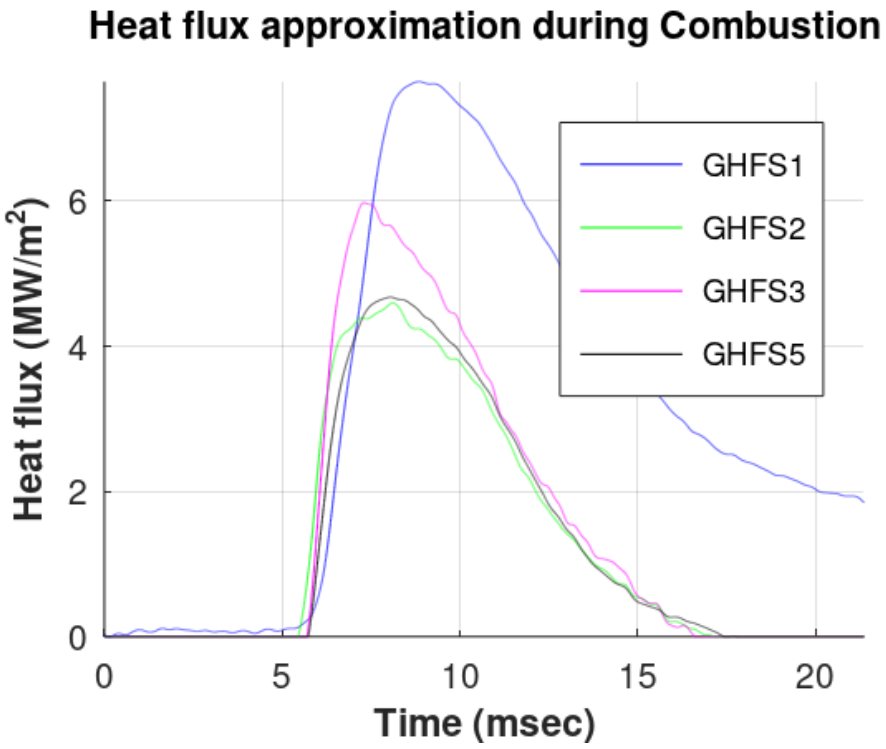


Figure 57. Heat flux approximation with constant sensitivity. Peak surface temperature was assumed to be 950K for all sensor positions.

The first scenario shows the peak heat flux being between 2.1 – 3.6 MW/m$^2$ while the second scenario measured 4.6 – 7.7 MW/m$^2$. The obtained values were within the same range as the estimated heat flux by the Wärtsilä CFD team (2021). Rough estimates being between 1 – 10 MW/m$^2$ and closer estimation between 5 – 10 MW/m$^2$. Similar range of heat flux was measured by Li et al. (1997) and Mahmud et al. (2021). The measured peak heat fluxes for both cases can be seen in Table 4.

Table 4. Estimated average peak heat flux with different surface peak temperatures in MW/m$^2$.

| | **Peak temperature 880 K** | **Peak temperature 950 K** |
|---|---|---|
| GHFS #1 | 3.54 | 7.64 |
| GHFS #2 | 2.13 | 4.60 |
| GHFS #3 | 2.77 | 5.98 |
| GHFS #5 | 2.16 | 4.68 |

# 5 Discussion

## 5.1 Sensor installation and design

Tests done with the instrumented corner module showed that the adhesive used to clamp GHFS to the sensor pit can prove to be a problem during combustion sequence due to pressure leakage. If the glue used would fail to seal the cable feedthrough it will cause pre-combustion sequence to stop since it has target pressure values in succession that needs to be achieved before it can continue. For example, during pressure and temperature tests done with an instrumented corner module inside, the OSCC had leakage issues. It was noticed that a leakage through the cable feedthrough made target vacuum pressure for the pre-combustion to be impossible. Thus, sealing the cable feedthrough with epoxy was needed to allow continuous measurement regardless of if the glued sensor would break or not. Furthermore, leakage is a good indicator that the used adhesive has failed.

The installed instrumented corner module showed that pre-combustion pressure waves would consistently break the adhesive layer connecting the GHFS and the corner module. Several combustion sequences were done during the validation tests done to the OSCC. When the instrumented corner module was installed for these tests, the adhesive layer broke from the first combustion sequence. Main cause for the breakdown of the adhesive layer was high pressure rise rate during pre-combustion. This mixture caused the ignition to resemble a detonation wave. Air–fuel ratio was changed to leaner mixture for instrumented plate test to lower pressure rise rate.

Sensor being broken was able to be seen from the measured signal recorded in Dewesoft. When the sensor broke, the signal showed negative values that would indicate negative heat flux inside the chamber. The signal would also fluctuate between positive and negative when outside the combustion sequence.

Noise was found in all the measurements. Noise was from the ground loop due to direct contact between the metal and the sensor. Failed instrumentation could be from the preparation quality done during pre-work. However, some issues found during instrumentation made the gluing process difficult. For example, the shape of the sensor not being square caused the mounting to the sensor pit to be not possible. Sensor pit area had to be widened to fit it for the sensor especially on the corners where solder joints were. Furthermore, placing the sensor wires through the cable route also caused problems with bending of the sensor. This caused issues when applying the adhesive layer to the sensor pit. Cable routes for the sensor were widened and deepened to limit this issue. Adhesive layer and solder joint were seen as the weakest link that broke during combustion sequences.

This can be seen from the sooty sensors collected after the measurements. Some of the adhesive material remains on the surface of the sensor on the opposite side of the cable route area. Soot was also seen on the cable route area. This indicated that the adhesive layer began to break from the solder joint corners. Other collected GHFS showed similar results. Due to machining done to the cable route and the corners the adhesive layer was exposed. Consecutive combustion sequences hitting the exposed side of the adhesive layer eventually broke it. Largest difference between the test done with the instrumented corner module and the instrumented plate was exposure to the pre-combustion detonation wave. For the instrumented corner module tests the detonation wave hit the adhesive layer directly. In comparison, due to the placement of the instrumented plate, the adhesive layer was not hit by the initial detonation wave. The adhesive layer eventually broke from repeated combustion sequences. Current instrumentation design is not able to survive testing inside the OSCC. Similar case can be expected if installed inside an engine combustion chamber. More robust design would be required before further testing is continued. Riiki (2021) suggests a design with a seal placed on top of the sensor. This would remove the possibility of the adhesive being exposed to the combustion sequence. For installation, a tightening nut would be required that would be used

after adding adhesive under and around the sensor. Design of the sensor installation is displayed Figure 58.

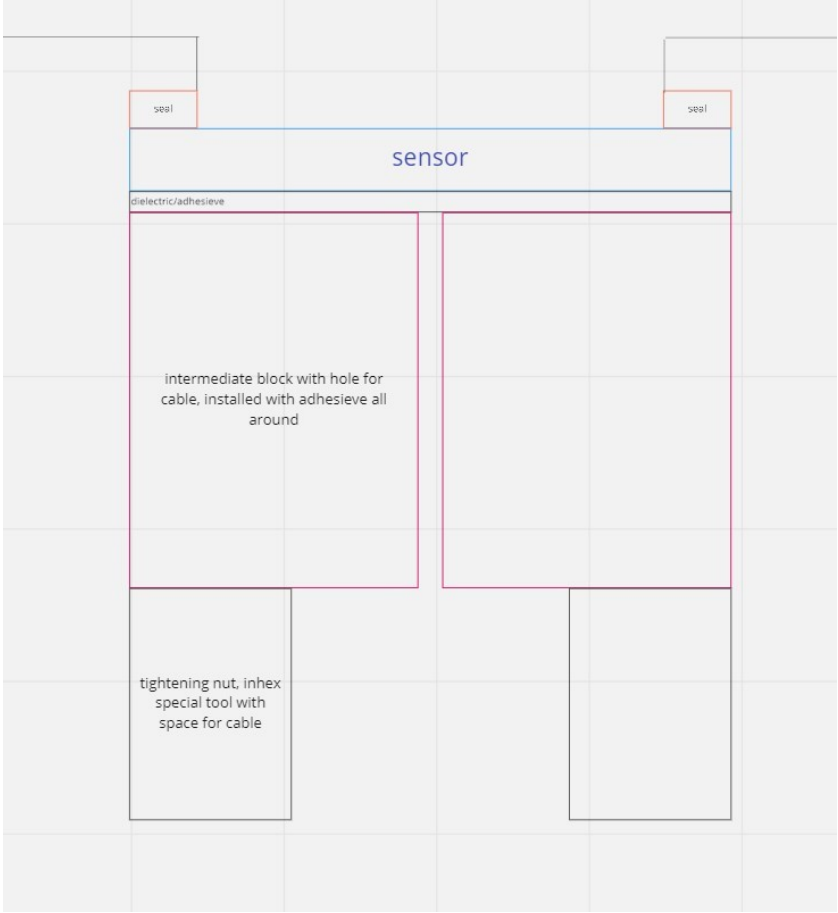


Figure 58. New design for sensor installation with robustness in mind. (Riiki, Sensor instrumentation improvements, 2021).

The high amount of noise from the ground loop indicated that the sensor was leaking either from direct contact between the sensor and metal or sensor wires and metal. Previously mentioned bended shape of the sensor during the placement could be one cause. The adhesive layer may have solidified under the sensor unevenly. Weight was placed to keep the sensor in place and straight, but some unevenness could be still possible. During the gluing process it is not possible to check if the installation is electrically isolated due to only achieving that after the gluing process is done. It is possible that the used Mega Cryl SST adhesive was a failed batch. It has happened before that defect batches have been received. It is recommended that for future installations other adhesive materials should be tested. Due to time constraints other adhesives were not tested

as originally planned. In addition, placement of sensor soldering joints should be reconsidered to lower bending caused when placing the sensor wires to the cable route. One example could be to place them on opposite corners to limit the bending.

The measured value GHFS signal was filtered due to noise from the ground loop. Although the noise caused a voltage drop from the signal, heat flux from the spray combustion caused a measurable voltage signal. This meant that it was possible to calculate estimation for heat flux during spray combustion. Mityakov (2021) states that although voltage drop was seen from the ground loop, it would be possible to recalibrate instrumented plates with sensors in place to have correct sensitivities for all sensors. Calibration would be similar as with only the sensor. Although it would not remove the noise, more accurate measurement of heat flux would be possible.

## 5.2 Instrumented plate measurement data

In total 30 combustion sequences were realized with the working installed GHFS. Of them, 15 combustion sprays were successful from which 11 were able to be used for further analysis. Last two successful sequences were not used due to breaking of sensors and the other two had differentiating fuel amounts that could not be used to calculate average signal for further analysis. Due to the noise seen on all instrumented sensor signals, sensitivities given for the sensor could not be used to measure heat flux on the surface of the instrumented plate. Thus, it was required to estimate the sensitivity of the sensor from estimating the peak surface temperature seen on the instrumented plate.

Different estimations presented were calculated that showed heat flux from combustion spray in different sensor positions. Peak heat flux was between 2.1 – 3.6 $MW/m^2$ or 4.6 – 7.7 $MW/m^2$ depending on the used peak surface temperature for sensors. From discussion with Wärtsilä the CFD team (2021) expected values were between 1 – 10 $MW/m^2$ with a closer estimation of between 5 – 10 $MW/m^2$. Similar range of heat flux was measured by Li et al. (1997) and Mahmud et al. (2021). Some uncertainty remains from setting limitations to calculate heat flux from sensitivity from surface temperature. Mityakov

(2021) notes that due to having sensitivity constant during the combustion sequence some inaccuracy is added to the measurement. More accurate representation of the sensitivity is that it changes as the surface temperature changes during the combustion sequence, reaching the lowest sensitivity during the peak temperature. Surface temperature that was used was measured at GHFS #3 position at 10.93 ms aSoE. Similar temperatures for all sensors were assumed to get estimations of heat flux but differences between temperatures should be expected.

Although noise was recorded on all signals, through filtering it was possible to record signals that showed the profile of heat flux in different sensor positions. For example, the highest heat flux was expected to be measured in the center of spray. Measured voltage signal showed that GHFS #1 had the highest voltage signal. When comparing these results to high-speed camera recordings, the area where GHFS #1 was placed the flame from combustion remains the longest. As new fuel is injected to the chamber and hitting the instrumented plate fuel is pushed away and moves to the corners of the plate. Due to the alignment block that places the instrumented plate perpendicular to the spray flame is not able to reach full radius from the center of the spray and starts spiraling in this region, causing the highest heat flux to be measured at GHFS #1. Average pyrometer data also shows this with two temperature peaks recorded. The first peak before the impingement of the flame onto the plate and secondary recorded by the pyrometer when the flame mushroom cloud reaches large enough shape (Sutton, ym., 2022).

# 6 Conclusion

Gradient Heat Flux Sensors (GHFS) were used to measure heat flux from a combustion spray. This was realized in an Optical Spray Combustion Chamber (OSCC) by replicating the conditions seen in an engine. A measurement campaign was performed to give validation data for CFD models. These models are used to analyze heat transfer in an internal combustion engine. Sensors were mounted inside the chamber onto a plate to limit complexity of the simulation model. Preparation work included testing the sensor installation durability inside the chamber before starting the measurement campaign. Parallel measurements were conducted to be used for further analysis. These included measurements with pyrometer, spectrometer, high–speed cameras and surface temperature measurement with phosphor thermometry. All data was synchronized with an injector control signal.

Results from the measurement campaign showed that the instrumentation method requires improvement. Sensor installation was only able to survive 30 consecutive combustion sequences, from which 15 had successful combustion sprays. Installation broke due to adhesive layer shattering. Another problem was with signal noise that came from unsuccessful electric isolation of the sensors. However, due to the strong heat flux from the spray combustion clear reaction was seen to the phenomenon from the measured voltage. The measured raw data was filtered for post-analysis. Signal noise made calibrations to the sensors obsolete. To improve the instrumentation method new design and testing of other adhesive materials was recommended.

Synchronization of data was successful between all the measurements. This allowed the usage of pyrometer and surface temperature of the plate for post-analysis. Measured surface temperature was used to recalibrate the sensors. This gave an approximation of the incoming heat flux during the combustion sequence. Peak heat flux was between 2.1 – 3.6 MW/m$^2$ or 4.6 – 7.7 MW/m$^2$ depending on the used peak surface temperature of the sensor. This correlated with the expected results of between 1 -10 MW/m$^2$ with closer estimations being between 5 – 10 MW/m$^2$.

# 7 Summary

Heat flux measurements were performed in an Optical Spray Combustion Chamber (OSCC) to give validation data for Conjugate Heat Transfer (CHT) analysis, conducted by the commissioner's CFD team. The chosen scenario was an injected spray combustion that would be similar to a W31 diesel spray inside the engine's combustion chamber. Only one of the injector nozzle's outlets would be used from the injector to simplify the experiment. Main measurement technique discussed in this thesis was Gradient Heat Flux Sensors (GHFS) that would allow high-speed speed measurement of heat flux from a whole combustion sequence. Same sensors have been tested inside the engine combustion chamber with problems seen in durability. Planning for instrumentation design and preparation work to install functional sensor mounting was discussed in this thesis.

Due to the difficulties in receiving valid measurement data with heat flux sensors inside an engine, some other environment was required. Thus, OSCC was used where conditions could be monitored and controlled to limit factors that the sensors would be exposed to. In addition, the amount of injected fuel could be chosen and aimed directly to the surface where sensors would be attached to. Due to the complexity required to simulate engine conditions with a CFD model, the OSCC also allowed simplifying the model. When designing a target surface, similar reasons were used to have a flat surface where injection spray would hit the sensors. Goal was that combustion spray would be hitting the plate perpendicularly. For the placement of sensors, the center point of the spray was chosen to be of interest. Three other sensors were placed the same length away from the center point to see if the same range value of heat flux could be seen from these sensors. Last sensor was placed even further away from the center point of the spray to see if diminishing heat flux could be seen from the sensor positions.

Preparation of sensor design was started with testing several adhesive materials to see how they would behave when exposed to heat and pressure. From these results, an adhesive material was chosen that would be used during experiments. When designing the instrumented corner module, the focus was to have a smooth surface when placing the

sensor to the sensor pit. Cable routes had to be machined deep enough that the sensor would not be elevated from the corner module. Cable routes were required for corners with solder joints to the sensor. Sensor pit area was fitted to the sensor to limit adhesive exposed to combustion. Adhesive layer was also kept minimal due to concerns that it would affect results measuring heat flux to surface metal.

After the preparation work, an instrumented corner module was tested inside the chamber during the validation of OSCC's hot combustion sequence. Initial issues were seen with leaking from cable feedthrough due to adhesive layer sealing it from the chamber. Modification was done to future instrumentation with using epoxy to seal cable feedthrough to limit chances of leakages during combustion sequence while instrumented components were installed. Sealed corner module was installed and was not able to survive the pre-combustion detonation wave, and no measurements of heat flux were able to be recorded. Another problem was with signal noise due to ground loop effect. Main cause was assumed to be either a direct contact between the sensor and metal or the adhesive layer not properly functioning as a protective layer for electrical isolation for the sensor.

During the alignment test other measurement devices were tested that would be used parallel to the GHFS during the final measurement campaign. These included a pyrometer, color and monochromatic high-speed camera and spectrometer. Pyrometer was able to measure flame spray temperature in an area from thermal radiance while high-speed cameras would be used for visual assistance. Pyrometer device testing was part of a DynPT project where new dynamic pressure and temperature measurements were studied. These measurements were synchronized with a master trigger signal which was a control signal for injection spray. Implementation of this was tested during the alignment test. In addition to these measurements, the instrumented plate was coated with phosphor to measure surface temperature in a specific time during a spray combustion sequence.

Results with the instrumented plate showed similar issues in noise but it was able to sustain 30 combustion sequences. These included 30 pre-combustions and 15 combustion sprays. From these 11 were able to be used to calculate an average heat flux. Due to the noise recorded on the measurement, the sensors had to be recalibrated. After these combustion sequences, broken sensors were collected for inspection that showed oxidation levels that would happen when exposed to temperatures over 875 K. Temperature measured by a Light Induced Phosphor gave an average of 880 K in the center of the spray. This was measured at approximately 11 ms after the Start of Energization of injector spray.

From measured temperatures an approximation of heat flux was calculated between 2.1 – 3.6 MW/$m^2$ or 4.6 – 7.7 MW/$m^2$ depending on the peak surface temperature assumed from the combustion sequence. Calculations assumed that sensitivity remains the same during the whole combustion sequence. Peak surface temperature was also assumed to be similar in all sensor positions. Expected heat flux was estimated to be around 1 – 10 MW/$m^2$ or closer to 5 – 10 MW/$m^2$.

Improvements for sensor mounting design were presented to have more durability. Main concern was the edges of the sensors where the adhesive layer would be exposed during combustion. Thus, sealing the layer around the sensor was optimal to remove the possibility of adhesive layer breaking from combustion. Furthermore, testing of adhesive materials not tested during the measurement campaign would be needed to see if noise issues or durability could be increased.

# References

Anatichuk, L. I. & Bulat, L. P. (2001). Poluprovodniki v ekstremalnikh temperaturnykh usloviyakh (Semiconductors in extreme temperature conditions). Saint-Petersburg. Nauka.

Baert, R., Frijters, P. J., Somers, L. M. & Lujiten, C. (2009). Design and Operation of a High Pressure, High Temperature Cell for HD Diesel Spray Diagnostics. Guidelines and Results. SAE Technical Papers. doi:10.4271/2009-01-0649.

Dewesoft. (2023). Sirius Technical reference manual v24-1. https://downloads.dewesoft.com/manuals/dewesoft-sirius-manual-en.pdf

Gerashchenko, O. A. (1971). Osnovy teplometrii (The basics of heat metering). Kiev. Naukova Dumka

Grahn, V. (2021). Evaluation of the Heat Transfer from the Diesel Spray Combustion in an Optical Spray Combustion Chamber. Vaasa. Åbo Akademi.

HBM (2022a). Soldering terminal how to https://www.hbm.com/en/8132/how-to-install-strain-gauges-video-tutorial/

HBM (2022b). Instructions for using cold curing adhesive x280. Retrieved 2022-4-15 from https://www.sensor-hbm.com/upload/product-file/a1657.pdf

HBM (2022c). Lead-Free Soldering of Strain Gauges. https://www.hbm.com/en/7781/lead-free-soldering-of-strain-gauges/

HBM (2024). Soldering Terminals for Strain Gauges. Retrieved 2024-4-15 from https://www.hbm.com/en/4629/strain-gauge-installation-solder-material/

Henkel (2014). Technical data sheet. Loctite EA 9492. Retrieved 2022-4-15 from http://tds.henkel.com/tds5/Studio/ShowPDF/?pid=EA%209492&format=MTR&subformat=HYS&language=EN&plant=WERCS

Heywood, J. B. (1988). *Internal Combustion Engine Fundamentals.* McGraw-Hill, Inc.

Koivuluoma, J. (2022). Automated Batch Testing System for an Optical Spray. Vaasa. Oulun yliopisto.

Kutz, M. (2013). Handbook of measurement in science and engineering (Vol. 1). Hoboken, NJ. Willey.

Kyowa (2022). Adhesives and Bonding Tools. Retrieved 2022-4-15 from https://www.kyowa-ei.com/eng/product/category/strain_gages/s_adhesive/index.html

Li, S., Kamimoto, T., Kobori, S., Enomoto Y. (1997). Heat Transfer From Impinging Diesel Flames to the Combustion Chamber Wall. SAE International. ISSN 01 48-7191

Mahmud, R., Kurisu, T., Ilminnafik, N., Nishida, K. (2021). Wall Heat Flux on Impinging Diesel Spray Flame: Effect of Hole Size and Rail Pressure at Similar Injection Rate Condition. SAE Technical Paper 2020-32-2313, 2020. doi:10.4271/2020-32-2313.

Mahmud, R., Kurisu, T., Nishida, K., Ogata, Y. (2019). Characteristics of Flat-Wall Impinging Spray Flame and Its Heat Transfer under Small Diesel Engine-Like Condition. 3rd Report: Effect of Oxygen Concentration. DOI:10.1088/1757-899X/462/1/012046

Mityakov, A. (2021a). Sensitivity recalibration for sensors. (P. Nyberg, Haastattelija)

Mityakov, A. (2021b). Sensor design and construction. (P. Nyberg, Haastattelija)

Mityakov, A. & Riiki, T. (2021). Planning of mounting GHFS to instrumented corner module and flat plate. (P. Nyberg, Haastattelija)

Riiki, T. (2014). Instrumentation work done for GHFS sensor plug installed to engine. (P. Nyberg, Haastattelija)

Riiki, T. (12 2021). Sensor instrumentation improvements. (P. Nyberg, Haastattelija)

Sapozhnikov, S. Z., Mityakov, V. Y., & Mityakov, V. A. (1998). Heat flux sensor for heat transfer investigation. 11th International Heat Transfer conference, 77-79.

Sapozhnikov, S., Mityakov, V, Mityakov, A. (2020). Heatmetry: The Science and Practice of Heat flux Measurement. https://doi.org/10.1007/978-3-030-40854-1

SpeedGoat. (2024). SpeedGoat test systems. Noudettu osoitteesta SpeedGoat Web site: https://www.speedgoat.com/solutions

Sutton, G.; Lowe, D.; Sposito, A.; Öster, A.; Grahn, V.; Nyberg, P.; . . . Leino, J. (2022). Validation of a fiber optic. PTB-Mitteilungen 4/2022, 83-105.

Van der Graaf, F. (1990). Heat flux sensors. In: Gopel (Ed.), “Thermal sensors” of the multivolume work “Sensors, a comprehensive series” (Chap. 8, Vol. 4).

Wärtsilä. (12 2021). Internal Presentation - Evaluation of Heat Transfer From Diesel Spray. (P. Nyberg, Haastattelija)

Wärtsilä Corporation. (2023). Products: Wärtsilä 31. Noudettu osoitteesta Wärtsilä Corporation Web Site: https://www.wartsila.com/marine/products/engines-and-generating-sets/dual-fuel-engines/wartsila-31

# Appendices

Appendix 1. Instrumented corner module design for GHFS mounting.

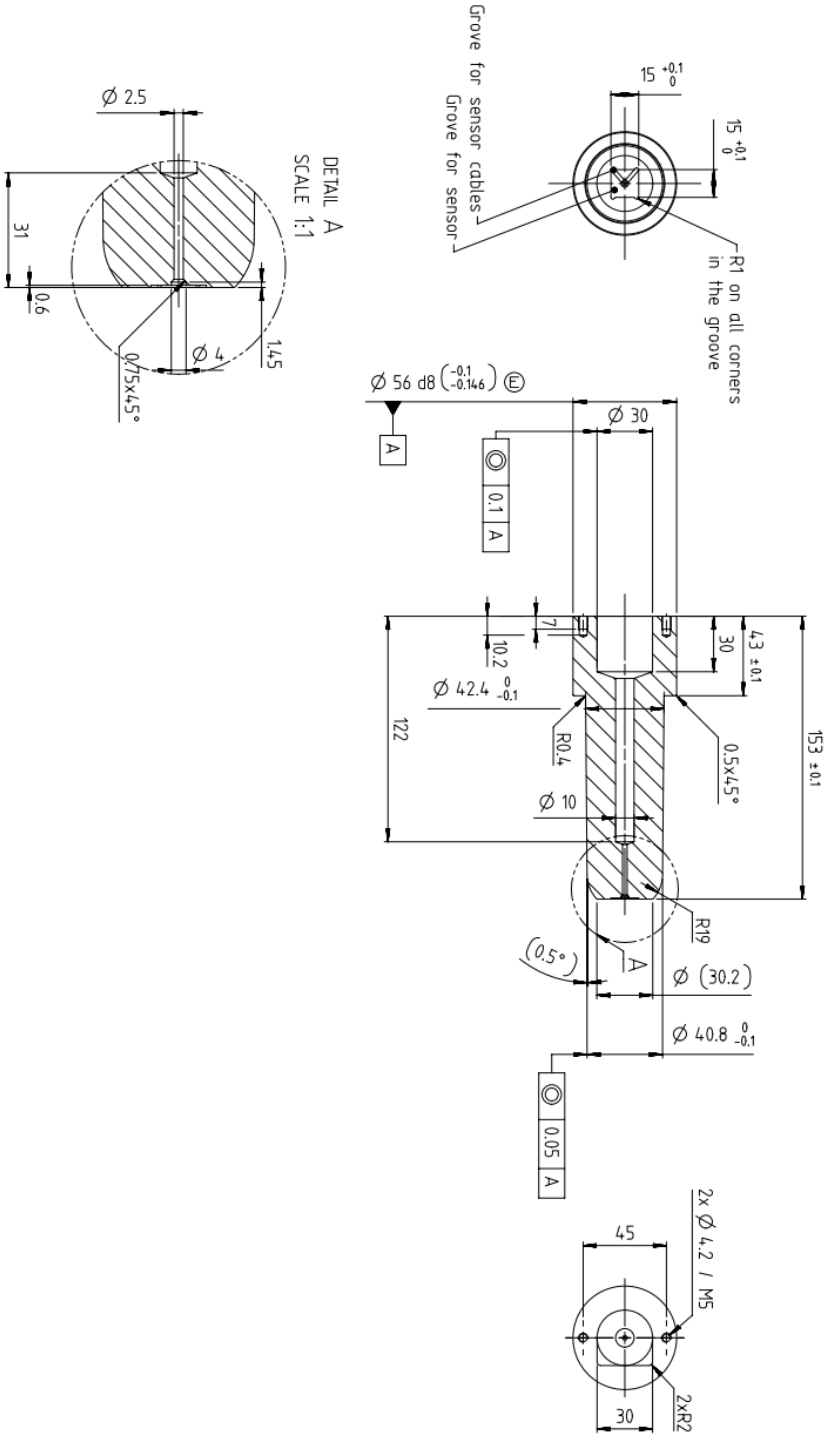

Appendix 2. Instrumented plate design for GHFS mounting.